Articular Surface Contact Parameters in High Tibial Osteotomy and Double Osteotomy: A Finite Element Approach

by

Raj Dhanush Srinivaasappa Indira

A thesis
presented to the University of Waterloo
in fulfillment of the
thesis requirement for the degree of
Master of Applied Science
in
Mechanical and Mechatronics Engineering

Waterloo, Ontario, Canada, 2024

© Raj Dhanush Srinivaasappa Indira 2024

Author's Declaration

I hereby declare that I am the sole author of this thesis. This is a true copy of the thesis, including any required final revisions, as accepted by my examiners.

I understand that my thesis may be made electronically available to the public.

Abstract

Osteoarthritis (OA) is a common joint disease characterized by the degeneration of articular cartilage, resulting in pain, stiffness, and reduced joint function. For knees affected with unicompartmental OA, High Tibial Osteotomy (HTO) is an effective surgical procedure to manage symptoms and slow disease progression. The surgery is performed by making an angled cut in the tibia and creating a wedge to realign the joint, shifting the load-bearing axis away from the affected compartment. For more severe deformities, a Double Osteotomy is performed, involving corrections in both the tibia and femur. These joint-preserving surgeries extend the life of the native knee and can often delay or prevent the need for partial or total knee replacement. Research indicates that the Medial Collateral Ligament (MCL) is strained during the osteotomy opening, which may lead to abnormal pressure distributions across the tibial plateau and affect the correction. However, it is unclear which osteotomy parameters influence this strain or the impact of additional or residual strain in the MCL on pressure distribution.

This study aims to develop knee finite element models to simulate various osteotomy correction angles, including uncorrected, optimal correction, and over-correction, for open-wedge HTO and double-level osteotomy to treat medial compartment OA. The primary goal is to investigate the contact force and pressure distribution across the tibial plateau at different simulated correction angles. Additionally, the study examines the strain in the MCL under various corrections to assess the effects of under-correction, optimal correction, and over-correction. A secondary objective is to evaluate the impact of partial and total release of the superficial MCL on force and pressure distributions across the tibial plateau. Finally, a double osteotomy procedure is simulated to determine contact parameters, with the results compared to those from HTO.

The osteotomy cuts were modeled on 3D models of the tibia and femur using SolidWorks, then exported and meshed in Hypermesh. The models were subsequently transferred to Abaqus CAE, where they were assembled with the other knee components. A distributed load of 800N at the proximal surface of the femur was applied and boundary conditions were provided at the hip and ankle joints. Non-linear static simulations were performed to determine the contact forces, pressures, and stress distributions across the tibial plateau. The superficial MCL was modeled as non-linear spring elements in Abaqus, and the force in the MCL was quantified for various corrections. Additionally, a gradual release of the superficial MCL was simulated by removing the spring elements from the model, and the resulting contact parameters were determined.

The results showed that the contact force on the medial compartment decreased by 3% for a 5° correction, while the contact force on the lateral compartment increased by

37%. A 20% rise in the contact force was observed on the medial tibial cartilage in the 7° correction model. Contact pressures in the medial compartment decreased with increasing correction angles and increased in the lateral compartment. A balanced distribution was noted at a 5° correction. The total MCL force increased from 187N in an uncorrected tibia to 410N in an overcorrected model, marking a 120% increase and causing a spike in the medial contact force for the overcorrected model. Reduction in medial compartment load distribution was observed after partial and total MCL release, suggesting that MCL release is a viable surgical option. For large corrections, double-level osteotomy offers a method to mitigate excessive stress on the medial compartment compared to a single osteotomy. The study demonstrated that FE models can be a useful tool for pre-planning procedures and predicting post-surgical outcomes.

Acknowledgements

I would like to express my deepest gratitude to my supervisor, Dr. Naveen Chandrashekar, and the University of Waterloo for providing me with the opportunity to pursue my master's degree. I am especially thankful to Dr. Chandrashekar for his invaluable insights, unwavering support, and continuous motivation. I thank Dr. Sebastian Tomescu (Sunnybrook Hospital) for his guidance throughout this project. His clinical expertise and experience were essential to my work.

I am grateful to Harish Raghavendra Rao for his support during this project and for assisting me with my queries. After all, his modeling efforts made this project possible and opened up possibilities for various other projects. My sincere thanks also go to my labmates, Mercy Ombogo, Anandita Gautam, and Howard Kao, and former labmates Raj Arjun Srinivaasappa Indira, Pratishta Gupta, and Dominic Tung, for their constant support and valuable insights into various aspects of this project, and for being great friends.

Lastly, I would like to thank my family and friends for their endless encouragement and support. I could not have achieved this without all of you.

Table of Contents

Author's Declaration ii

Abstract iii

Acknowledgements v

List of Figures ix

List of Tables xii

1 Introduction 1

1.1 Motivation 1

1.2 Objectives 2

1.3 Thesis Overview 3

2 Background and Literature Review 4

2.1 Anatomical Background 4

2.1.1 Nomenclature 4

2.1.2 Lower Limb Anatomy 6

2.1.3 Knee Anatomy 7

2.2 Knee Osteoarthritis 12

2.2.1 Varus and Valgus malalignment 13

2.2.2 Clinical Interventions . . . 14
2.3 High Tibial Osteotomy . . . 15
2.3.1 Surgical Technique . . . 15
2.3.2 Clinical Outcomes . . . 17
2.4 Experimental Studies . . . 19
2.5 Finite Element Studies of HTO . . . 23
2.5.1 FE studies of HTO procedure . . . 23
2.6 Summary . . . 24
2.7 Hypothesis . . . 24

3 Methodology **26**
3.1 Development of Finite Element Model . . . 26
3.1.1 Finite Element Knee Model Origin . . . 26
3.1.2 Pre-planning procedure . . . 29
3.1.3 Surgical Simulation of HTO . . . 32
3.1.4 Double Osteotomy model generation . . . 34
3.1.5 Meshing of the bones and soft tissues . . . 35
3.2 Finite Element Analysis . . . 36
3.2.1 Loading and Boundary conditions . . . 36
3.2.2 Validation of FE model . . . 38
3.2.3 MCL Release . . . 38
3.3 Contact Outputs and Summary . . . 39

4 Results **41**
4.1 Mesh Quality Assessment . . . 42
4.2 Effect of Correction Angle on Articular Surface Contact Forces . . . 43
4.3 Effect of Correction Angle on Articular Surface Peak Contact Pressures . . . 45
4.4 Effect of Correction Angle on the stress distribution across the articular surface . . . 50

4.5 Effect of Correction Angle on MCL Strain . . . 53
4.6 Effect of Release of the Superficial MCL on the Articular Surface Contact Force, and Pressure distributions . . . 54
4.7 Results of Double Osteotomy . . . 57

5 Discussion **61**
5.1 Development of FE Model . . . 61
5.2 Finite Element Analysis . . . 62
5.2.1 Validation of FE model . . . 62
5.2.2 Effect of varying correction angle on the articular surface and MCL strain . . . 63
5.2.3 Effect of MCL Release on articular surface force and pressure distributions . . . 67
5.2.4 Double Osteotomy . . . 69
5.3 Significance of current study . . . 70

6 Conclusions **72**
6.1 Summary . . . 72
6.2 Limitations and Future Work . . . 73

References **75**

List of Figures

2.1 Anatomical Planes and Directional Pairs 5
2.2 Lower Limb Anatomy 6
2.3 Knee Joint Anatomy 8
2.4 Structure of Articular Cartilage 11
2.5 Normal knee vs Knee with OA 12
2.6 Lower Limb Alignment 14
2.7 Fujisawa point 16
2.8 Opening Wedge High Tibial Osteotomy. A) A guide wire is placed 3.5-4 cm below the medial joint line to about 1 cm below the lateral articular margin of the tibia B) Osteotomy performed with an oscillating saw C) Medial tibia opened with a wedge 17
2.9 (a) Synthetic insert with fixation plate (b) Fixation plate only 20
2.10 Cadaveric knee specimen, mounted into the testing fixture 22

3.1 Overview of steps involved in the development of FE model 26
3.2 Knee segmentation from MRI scans on 3D Slicer 27
3.3 Digitization process of ligament insertion 28
3.4 (a) Cadaver specimen (Adapted from [72]) (b) 3D model of the knee joint . 30
3.5 Pre-planning procedure for HTO 31
3.6 Tibia split into two parts by defining cutting axis 32
3.7 Removal of the wedge on the lateral side of the tibia 33

3.8 (a) Uncorrected tibia model (b) Tibia with an osteotomy wedge cut and opening (c) Wedge filled with graft 33
3.9 (a) Uncorrected femur model marked with correction angle (b) Removal of wedge from the lateral side (c) Wedge closed to simulate distal femoral osteotomy 34
3.10 Tetrahedral meshes of the bones 35
3.11 Distributed load of 800N on femur 36
3.12 Frontal and Sagittal plane motion allowed at hip and ankle joints based on Agneskirchner et al [2] 37
3.13 Partial and total release of Superficial MCL 39

4.1 Orientation of Contour plots (a) Orientation of femoral cartilage (b) Orientation of medial and lateral tibial cartilages 41
4.2 Contact forces results at surface pairs for different correction angles 43
4.3 Contact force distribution on the femoral cartilage 44
4.4 Contact force distribution on the proximal surface of medial tibial cartilage 44
4.5 Contact force distribution on the proximal surface of lateral tibial cartilage 45
4.6 Contact Pressures at the medial compartment for different correction angles 46
4.7 Contact Pressures at the lateral compartment for different correction angles 46
4.8 Contact Pressure distribution on the femoral cartilage 47
4.9 Contact Pressure distribution on the proximal surface of lateral tibial cartilage 48
4.10 Contact Pressure distribution on the proximal surface of medial tibial cartilage 49
4.11 Von Mises stresses at the medial compartment for different correction angles 50
4.12 Von Mises stresses at the lateral compartment for different correction angles 51
4.13 Von Mises stress distribution on the femoral cartilage 51
4.14 Von Mises stress distribution on the proximal surface of lateral tibial cartilage 52
4.15 Von Mises stress distribution on the proximal surface of medial tibial cartilage 52
4.16 Effect of Correction Angle on Force in MCL 53
4.17 Effect of MCL release on Contact Force between surface pairs 55

4.18 Effect of MCL release on Contact Pressure distribution across the medial compartment for 5° correction 55
4.19 Effect of MCL release on Contact Pressure distribution across the lateral compartment for 5° correction 56
4.20 Contact Force comparison between HTO at 7° correction and Double Osteotomy 58
4.21 Contact Pressure comparison between HTO at 7° correction and Double Osteotomy on the medial compartment 59
4.22 Contact Pressure comparison between HTO at 7° correction and Double Osteotomy on the lateral compartment 59
4.23 Von Mises Stress comparison between HTO at 7° correction and Double Osteotomy on the medial compartment 60
4.24 Von Mises Stress comparison between HTO at 7° correction and Double Osteotomy on the lateral compartment 60

5.1 Geometry of medial tibial cartilage and load distribution on 7° correction . 64
5.2 Change in contact area in medial and lateral compartments 64
5.3 Comparison between contact pressure on the medial and lateral compartments for MCL release conditions 68

List of Tables

2.1 Studies reporting survivorship of HTO 18

3.1 Ligament bundles used in the FE model (Adapted from [72]) 29
3.2 Material property data for bones and soft tissues 29
3.3 Summary of FE models developed 40

4.1 Mesh Metrics 42
4.2 Shape Metrics 42
4.3 Contact forces between articular surface pairs for different corrections . . . 43
4.4 Contact pressures on the articular surface for different corrections 45
4.5 Stress distribution across the articular surface for different corrections . . . 50
4.6 Contact forces between articular surface pairs due to partial and total MCL release. The numbers represent contact forces in Newtons (N). 54
4.7 Contact pressures on the articular surface as a result of partial and total MCL release 54
4.8 Contact Force comparison between HTO at 7° correction and Double Osteotomy 57
4.9 Contact Pressure comparison between HTO at 7° correction and Double Osteotomy 57
4.10 Von Mises Stress comparison between HTO at 7° correction and Double Osteotomy 58

Chapter 1

Introduction

1.1 Motivation

Osteoarthritis (OA) is a prevalent degenerative joint disease characterized by the breakdown of cartilage, leading to pain, stiffness, and reduced joint function. The socioeconomic impact of OA is significant, contributing to escalating healthcare costs due to medical interventions and affecting workplace productivity. According to the National Report on the Status of Arthritis of Canada (2019), about 6 million people were affected with osteoarthritis, representing 20% of the Canadian population [8]. The numbers are estimated to increase to 8.8 million by 2040. As of 2020, the total economic burden of OA was approximately $405 billion [12]. The knee accounts for 83% of the total OA disability burden and is by far the most incapacitating type of OA [47].

Contrary to the traditional understanding of OA as a wear and tear disease, it is now understood to be multi-factorial, and the biomechanics of the knee joint is among the most critical factors in its pathogenesis [35]. A significant contributor to the aberrant loading of the knee joint is the malalignment of the tibia and femur [19]. The knee joint alignment is defined by the load-bearing axis of the lower limb – a line drawn from the center of the femoral head to the center of the talus. On average, the load-bearing axis passes through a point approximately 4 ± 2 mm lateral to the center of the knee joint [49]. In a varus deformity (bow-legged), the load-bearing axis crosses medial to this point, while falling laterally in a patient with valgus deformity (knock-knees). A shift in the load-bearing axis leads to abnormal pressure distributions across the tibial plateau resulting in uni-compartmental osteoarthritis.

For knees affected with medial compartment OA progression, an opening wedge high tibial osteotomy (HTO) can be an effective intervention to manage symptoms of OA [83]. Knee osteotomies are performed by making an angulated cut in the tibia and creating a wedge that realigns the joint and shifts the load-bearing axis away from the affected compartment. For more severe deformities, a Double Osteotomy is suggested, involving corrections in both the tibia and femur [7, 60]. Research suggests that the Medial Collateral Ligament (MCL) is strained and pressure is abnormally distributed on the tibial plateau [86]. However, there is a lack of consensus on the parameters that affect this strain and its relationship with contact parameters over the articular surface.

Knee osteotomies have a multi-factorial etiology making it complex to research with traditional clinical methods. Computational tools, such as Finite Element Models, can be highly effective for planning surgical procedures and predicting outcomes. Several studies have highlighted the importance of simulating osteotomy procedures to analyze load and pressure patterns on the knee joint. Despite this, many computational methods haven't yet produced better outcomes than traditional techniques due to their lack of outcome prediction and consideration of biomechanical characteristics. The present study employs a more clinically relevant approach to develop finite element models to simulate the surgical procedure. Moreover, the procedure adopted emulates a healed knee after HTO, which is crucial for the analysis of post-operative conditions. In a healed state, the bone at the osteotomy site has fully integrated, with its mechanical properties restored, and the mechanical properties of the graft emulate those of the bone. This accurately represents the long-term outcomes and stability of the correction. The study aims to determine the effects of the surgery on articular surface contact parameters, specifically the contact forces, pressures, and stress distributions across the articular surface. The study also aims to quantify the influence of the MCL on the surgical procedure and its implications, which is yet to be investigated computationally. Studies have yet to computationally quantify the efficacy of double osteotomy compared to single osteotomy, and this study aims to address that gap.

1.2 Objectives

The primary objective of this study is to investigate the contact force and pressure distribution across the tibial plateau at various simulated osteotomy correction angles. The specific objectives were:

1. Develop knee finite element models at various osteotomy correction angles for open-wedged high tibial osteotomy and double osteotomy.

2. Determine the tibiofemoral contact force and pressure distribution across the tibial plateau and MCL strain for under-correction, optimal correction, and over-correction.

3. Investigate the effect of the release of the superficial MCL on the pressure distribution across the tibial plateau.

4. Investigate contact parameters for a double-level osteotomy and compare the results with a single-level osteotomy.

1.3 Thesis Overview

The thesis is organized into the following chapters. Chapter 1 (Introduction) sets the premise for the research conducted, including the motivation and objectives. Chapter 2 (Background and Literature Review) provides an overview of the lower limb anatomy, mechanics of osteoarthritis and clinical interventions, past and current clinical and biomechanical studies of the human knee, clinical and biomechanical studies conducted on high tibial osteotomy including FE models. The chapter concludes with a brief description of the gap in current studies and hypotheses for the current research. Chapter 3 (Methodology) is divided into two primary sections. The first section discusses the development of a FE model of the human knee to emulate HTO and double osteotomy surgical procedures, including mesh generation. The second section focuses on the overall FE study of the current research, encompassing FE model setup, material property definition, and analyses performed to meet the aforementioned objectives. Chapter 4 (Results) discusses the results of the study, which comprises mesh quality, articular surface contact parameters, MCL strain, consequences of the release of MCL, and results of double osteotomy. Chapter 5 (Discussion) analyzes the results in comparison to existing studies in the literature. Chapter 6 (Conclusions) presents the primary conclusions of the research, discusses the study's limitations, and suggests potential directions for future research.

Chapter 2

Background and Literature Review

2.1 Anatomical Background

A thorough comprehension of the human lower limb and knee anatomy serves as a foundational prerequisite for the application of engineering principles. This facilitates a comprehensive understanding of the complex mechanics underlying the pathogenesis and progression of osteoarthritis. The subsequent sections provide an overview of anatomical nomenclature, lower limb, and knee-specific anatomy.

2.1.1 Nomenclature

The anatomic planes are based on three primary planes: the *sagittal*, *frontal*, and *transverse* planes. The sagittal plane divides the body into left and right halves, with movements within this plane typically characterized as *flexion* or *extension*. The frontal plane bisects the body into front and back halves, with movements described as *abduction* or *adduction*. The transverse plane separates the upper and lower body segments, and movements within this plane are often classified as *internal/external rotation* or *pronation/supination*.

In addition, a series of directional pairs are utilized to denote the relative position of anatomical structures. These include *anterior-posterior* (towards the front or back), *superior-inferior* (towards the head or feet), *medial-lateral* (towards or away from the body's midline), *proximal-distal* (closer to or further from the torso), and *superficial-deep* (towards or away from the skin surface) (Figure 2.1).

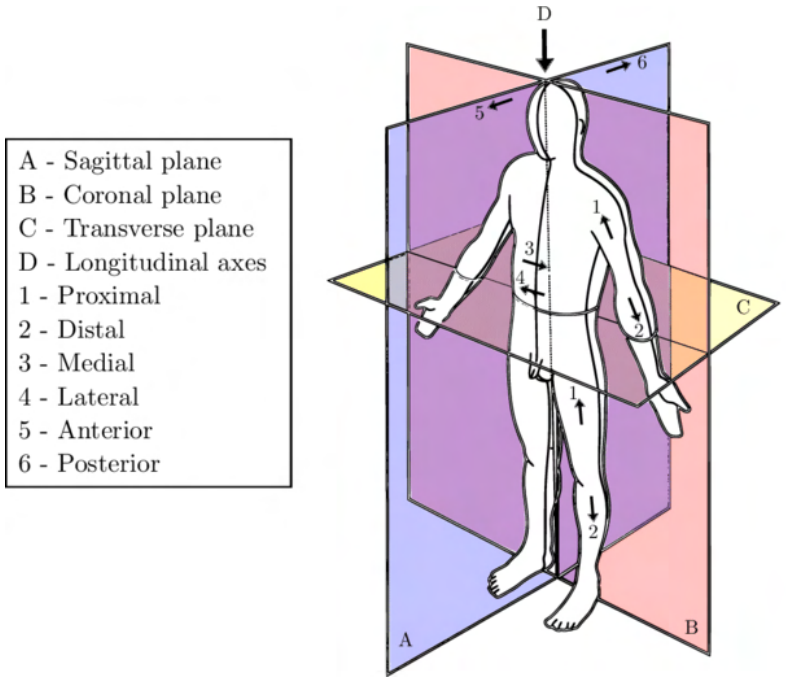


Figure 2.1: Anatomical Planes and Directional Pairs
(Adapted from [75])

A *joint* is a region where the ends of two bones meet. Joints can be categorized based on the nature of the union between the constituent bones and can be classified as *synovial*, *fibrous*, or *cartilaginous* in nature [57].

In the case of synovial joints, the entire articulation is encapsulated within a specialized joint capsule. The end surfaces of the adjoining bones are covered with a layer of articular cartilage, and the interior of the joint capsule is lubricated by synovial fluid. Synovial joints exhibit an extensive range of motion compared to other joint types, with their movement constrained by the presence of ligaments within the joint capsule. Examples of the synovial joints include the shoulder, knee, hip, hand, wrist, C1 and C2 vertebrae.

Fibrous and cartilaginous joints are distinguished by the presence of fibrous or cartilaginous tissue connecting the bones, resulting in either no movement or a limited range of motion. Fibrous joints are found between the bones of the skull, while cartilaginous joints are found between intervertebral discs.

2.1.2 Lower Limb Anatomy

The lower limb comprises four parts: *hip*, *thigh*, *leg*, and *foot* as shown in Figure 2.2. The hip is formed by the articulation of the *femoral head* (hip bone) and *acetabulum* of the *pelvic girdle* (socket). The hip joint serves as the primary connection between the lower limb and the vertebral column, facilitating weight transfer from the trunk to the lower limb. *Thigh* comprises the *femur* (thigh bone), which connects the hip and knee joints; and the *patella* (knee cap) on the anterior surface of the knee. Leg, the region between the knee and ankle consists of two bones, the tibia and fibula. *Foot* is the distal part of the lower limb connected to the leg by an ankle joint consisting of the tarsal bones. The foot includes metatarsals and their respective phalanges.

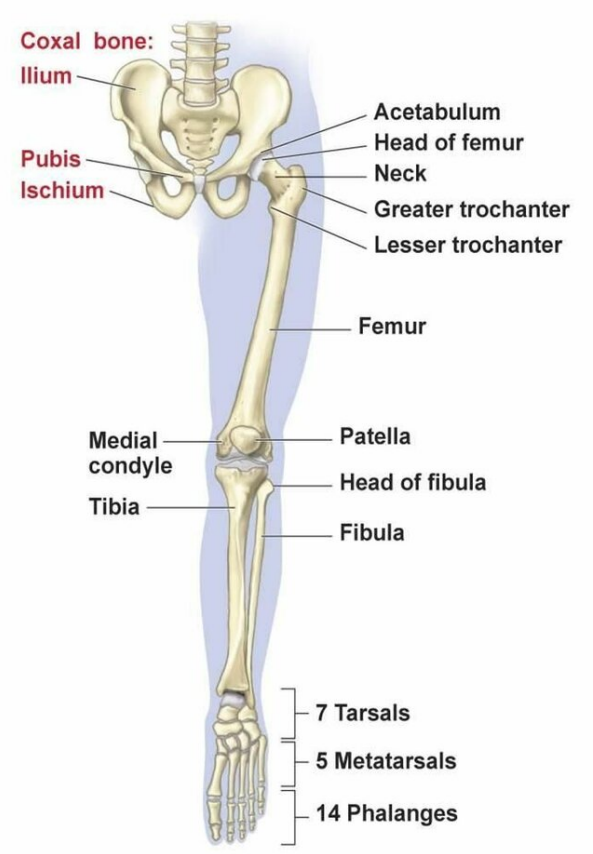


Figure 2.2: Lower Limb Anatomy
(Adapted from [59])

The lower limb is specialized to support body weight, maintain equilibrium, and locomotion [57]. Among its key roles, the lower limb supports the body's weight and transfers the gravitational load to the axial skeleton. The weight-bearing function is augmented by the pelvic girdle, which anchors the lower limb to the axial skeleton. The robust framework of the bony structures, in conjunction with the stability of hip, knee, and ankle joints enables efficient transmission of forces from the trunk to the ground.

2.1.3 Knee Anatomy

The knee joint is the largest synovial joint in the body and facilitates flexion, extension, and small rotations when flexed [33]. The musculoskeletal components that make up the knee joint are categorized into three groups: bones, ligaments, and cartilage, as shown in Figure 2.3.

The union of three bones forms the knee joint: *femur*, *tibia*, and *patella*. The ends of each of these bones are layered by articular cartilage, creating a lubricated, low-friction environment for load transmission between bones. The fibula is not involved in the knee joint and is laterally attached to the tibia.

The knee joint is composed of two main articulations: the *tibiofemoral joint*, the joint between the tibia and the femur, and the *patellofemoral joint*, the joint between the patella and the femur. The patellofemoral joint acts as an additional moment arm for the quadriceps muscles, allowing them to generate greater forces to extend the knee. The patella functions as a lever, enabling the quadriceps tendon to exert pulling forces on the tibia more effectively. The *patellar tendon* connects the distal end of the patella to the *tibial tuberosity*, a bony prominence on the tibia. The tibiofemoral joint supports the axial (vertical) loads experienced due to *ground reaction forces* (GRF) during activities like walking, running, and jumping. This joint helps absorb the impact and stress of these dynamic movements.

Knee Ligaments

The ligaments of the knee joint can be divided into two groups: *extracapsular* and *intracapsular* [57]. These ligaments connect the femur and tibia, providing stability to the knee joint, and preventing dislocation.

Five extracapsular ligaments strengthen the joint capsule: the patellar ligament, fibular (lateral) and tibial (medial) collateral ligaments, and oblique and arcuate popliteal liga-

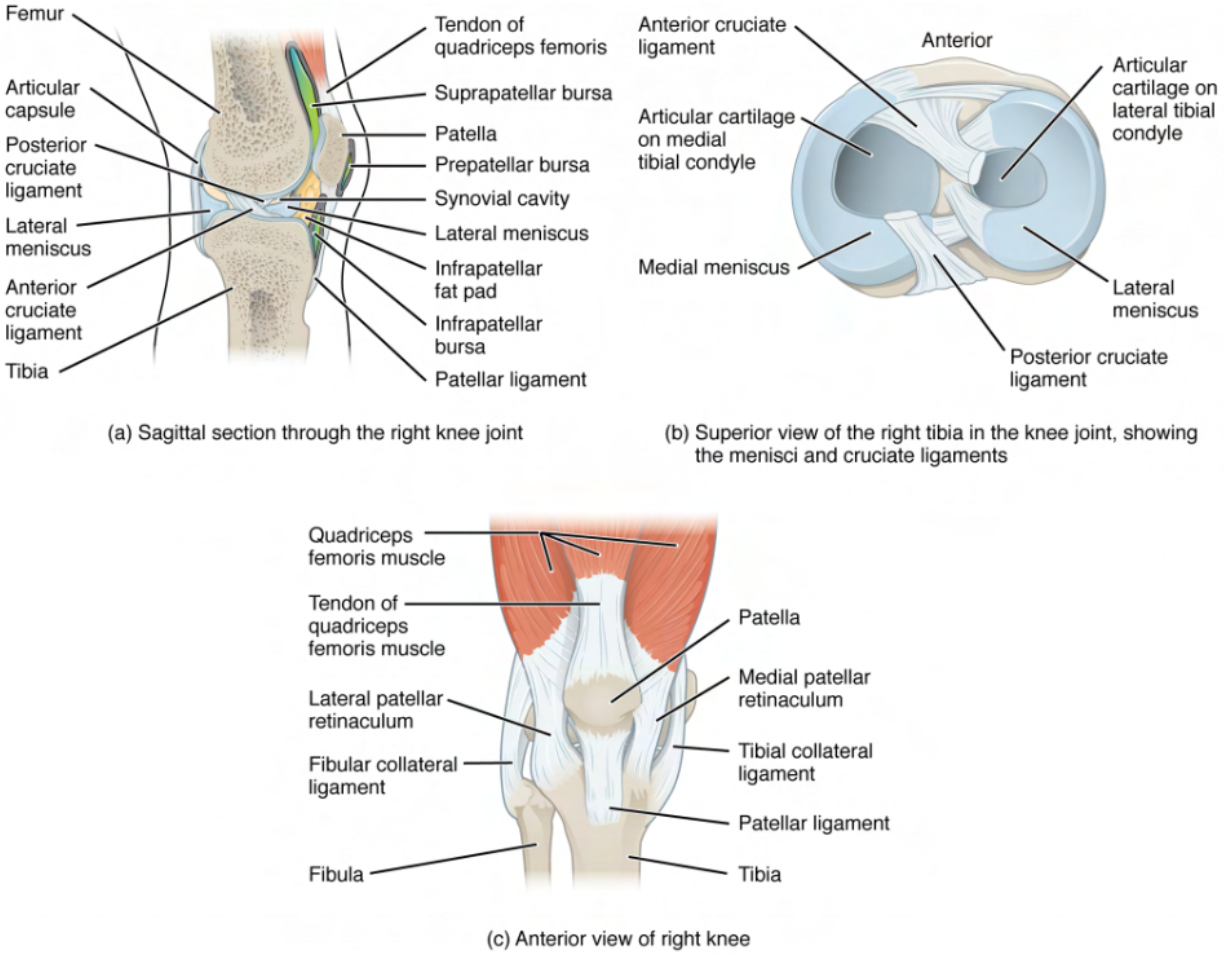


Figure 2.3: Knee Joint Anatomy
(Adapted from [1])

ments. Intracapsular ligaments, the anterior and posterior cruciate ligaments, are found inside the joint capsule.

Extracapsular Ligaments

The *patellar ligament* is a strong, thick fibrous band that is the distal part of the quadriceps tendon. It is found anterior to the infrapatellar bursa and extends from the apex of the patella to the tibial tuberosity. Along its outer margins, the patellar ligament blends with the medial and lateral patellar retinacula, which are extensions of the vastus medialis and lateralis muscles, and the overlying fascia. The patellar ligament plays a major role in stabilizing the patella and preventing its displacement.

The *fibular (lateral) collateral ligament* (LCL) is a strong ligament that extends inferiorly from the lateral epicondyle of the femur and extends distally to attach to the lateral surface of the head of the fibula. The LCL is found deep to the lateral patellar retinaculum, and superficial to the tendon of popliteus muscle, which separates the ligament from the lateral meniscus. The ligament also splits the tendon of the biceps femoris muscle in two.

The *tibial (medial) collateral ligament* (MCL) is a strong, flat ligament of the medial aspect of the knee joint that extends from the medial epicondyle of the femur to the medial condyle of the tibia. The MCL, in addition to its lateral counterpart, secures the knee joint and prevents excessive sideways movement by restricting external and internal rotation of the extended knee. The MCL is divided into *superficial* and *deep* parts:

The superficial part originates proximal to the medial epicondyle of the femur. This ligament has two attachment points: a proximal attachment on the medial condyle of the tibia, and a distal attachment on the medial shaft. Anteriorly, the superficial part blends with the medial patellar retinaculum and the medial patellofemoral ligament, which courses from the medial femoral condyle to attach onto the medial border of the patella. The deep part is found underneath the superficial part of the MCL and is a vertical thickening of the knee joint capsule. It originates from the area of the distal femur, then attaches to the medial meniscus, and terminates on the proximal tibia.

The *oblique popliteal ligament* is a thickening of the posterior capsule of the knee joint. It originates from the posterior aspect of the femur, above the articular surface, and inserts on the posterior aspect of the proximal tibia. This ligament helps to reinforce the posterior aspect of the knee joint capsule.

The *arcuate popliteal ligament*, also known as the arcuate ligament, is a U-shaped band of fibers that originates from the posterior aspect of the proximal tibia, lateral to the

insertion of the posterior cruciate ligament. It then courses superolaterally around the posterior aspect of the knee joint, inserting on the styloid process of the fibula. This ligament helps to reinforce the posterolateral corner of the knee joint.

Intracapsular Ligaments

The knee joint contains two main intracapsular ligaments - the *anterior cruciate ligament* (ACL) and the *posterior cruciate ligament* (PCL). These ligaments are located within the knee joint capsule.

The *anterior cruciate ligament* is the weaker of the two cruciate ligaments and originates from the posterior aspect of the anterior intercondylar area of the tibia and courses superiorly, posteriorly, and laterally to insert on the medial aspect of the lateral femoral condyle. The ACL helps prevent anterior translation of the tibia relative to the femur and limits hyperextension of the knee.

The *posterior cruciate ligament* originates from the posterior intercondylar area of the tibia and courses anteriorly, superiorly, and medially to insert on the lateral aspect of the medial femoral condyle. The PCL restrains posterior displacement of the tibia and limits excessive flexion of the knee joint.

Articular Cartilage

Articular cartilage is a highly specialized form of hyaline cartilage that covers the articulating surfaces of bones in diarthrodial joints [15]. This tissue plays a critical role in joint function, providing a smooth, slippery surface that facilitates the efficient transmission of mechanical loads with minimal friction during articulation. The knee joint consists of three primary cartilages. The femoral cartilage, tibial cartilage, and the patellar cartilage. The femoral cartilage rests on the femoral condyle, the tibial cartilage covers the tibial plateau, and the patellar cartilage lies on the posterior surface of the patella.

The thickness of articular cartilage typically ranges from 2 to 4 millimeters [29] and unlike most other tissues, they do not have blood vessels, nerves, or lymphatics. The *extracellular matrix* (ECM) of articular cartilage is the primary structural and functional component of this tissue. ECM is composed primarily of water, collagen, and proteoglycans, as well as a variety of other non-collagenous proteins and glycoproteins [14]. The collagen fibrils, which are predominantly type II collagen, provide the tissue with its tensile strength and resistance to shear forces, while the proteoglycans, such as aggrecan, confer its ability to withstand compressive loads.

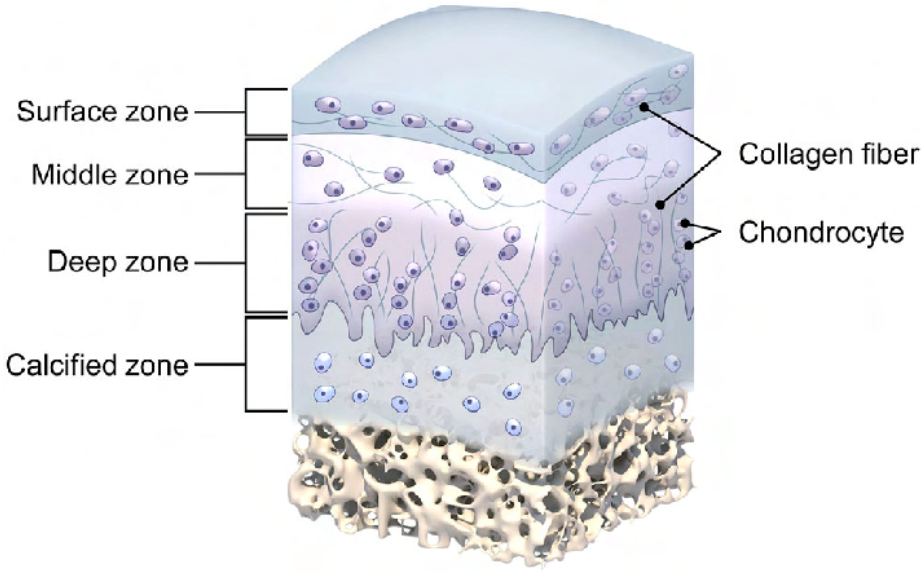


Figure 2.4: Structure of Articular Cartilage
(Adapted from [91])

Chondrocytes are specialized cells found in articular cartilage that are crucial for maintaining the structure and function of cartilage by producing and regulating ECM components. These cells originate from mesenchymal stem cells and undergo a series of differentiation steps to become mature chondrocytes. Chondrocytes are highly responsive to biomechanical signals and play a role in cartilage repair and homeostasis. However, they have a limited capacity for regeneration, which can be prone to degenerative joint diseases such as osteoarthritis when the cartilage is damaged [35].

Articular cartilage exhibits a distinct zonal organization, with four identifiable layers or zones: the superficial/surface zone, the middle zone, the deep zone, and the calcified zone, as shown in Figure 2.4. Each zone possesses unique characteristics in terms of collagen fiber orientation, proteoglycan content, and chondrocyte morphology, all of which contribute to the tissue's overall mechanical properties. The superficial zone, which is in direct contact with the joint cavity, protects the deeper layers from shear stresses and provides tensile properties. The middle zone resists compressive forces, while the deep zone offers the greatest resistance to compression. The calcified zone serves to anchor the articular cartilage to the underlying subchondral bone.

2.2 Knee Osteoarthritis

Knee osteoarthritis (OA) is characterized by the breakdown and progressive deterioration of the articular cartilage causing pain, stiffness, and impaired function. As the disease progresses, the knee joint is prone to uneven cartilage erosion, subchondral bone remodeling, and osteophyte formation [39, 90] (Figure 2.5). OA has a multi-factorial etiology and can be considered the product of an interplay between systemic and local factors [92]. Key risk factors include aging, gender, obesity, previous joint-related injuries, genetics, and chronic mechanical stress from physical activities [20, 48].

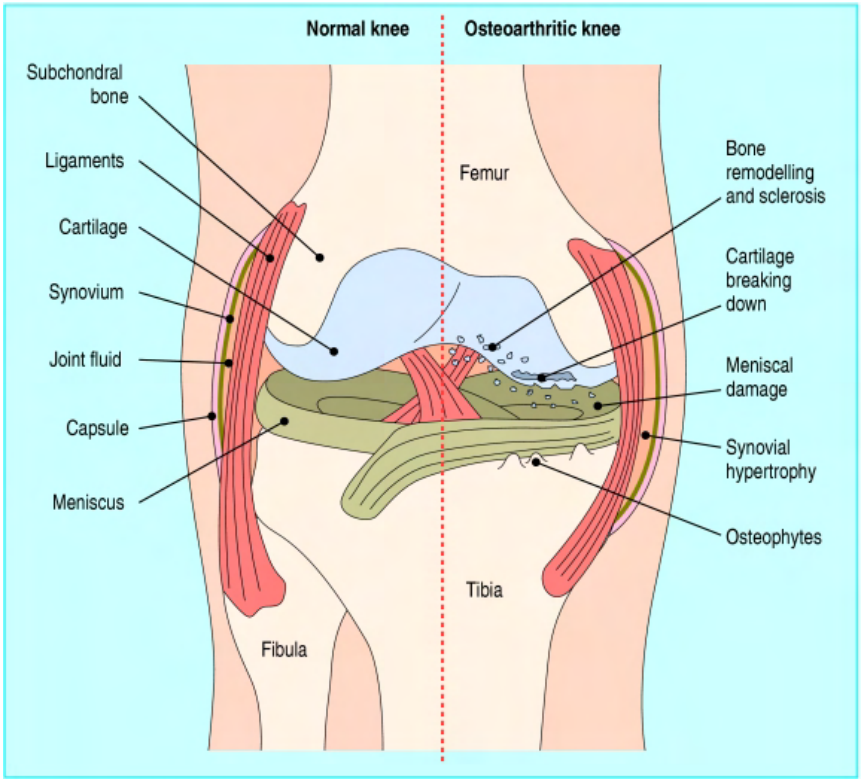


Figure 2.5: Normal knee vs Knee with OA
(Adapted from [39])

The biomechanics of OA is amongst the most critical factors in the pathogenesis of the disease [35]. The mechanical properties of the articular cartilage depend on the extracellular matrix components organized into an ordered molecular framework by the chondrocytes. Chondrocytes are highly responsive to biomechanical signals and are crucial for cartilage

repair and homeostasis. Their survival depends on optimal chemical and mechanical environments. Due to their limited potential for healing, failure of chondrocytes in homeostasis triggers OA progression [29, 35]. Factors such as joint instability, malalignment, and excessive or aberrant mechanical loading disrupt the normal mechanotransduction pathways in chondrocytes, making them unable to sense and adequately respond to abnormal biomechanical stimuli. This disrupts homeostasis, increasing matrix-degrading enzymes and decreasing structural matrix components. This progressive cartilage degeneration worsens chondrocyte dysfunction, accelerating OA progression.

2.2.1 Varus and Valgus malalignment

Malalignment of the lower limb significantly contributes to the onset and progression of OA [19], by significantly impacting the load distribution on the knee joint. Knee joint alignment is quantified by the *hip knee angle* (HKA), which is the angle formed at the knee joint center between the mechanical axes of the femur (FM) and tibia (TM) (Figure 2.6). The mechanical axis of the femur is a line drawn from the center of the hip joint to the knee joint center, and the mechanical axis of the tibia is drawn from the knee joint center to the center of the talus. The *mechanical* or *load-bearing axis* (LBA) of the lower limb is drawn from the center of the femoral head to the center of the talus. For a healthy knee, the load-bearing axis passes through a point approximately 4±2 mm lateral to the center of the knee joint [49], or 2°– 3° of varus compared with the mechanical axis [77].

Lower limb malalignment refers to a deviation from the normal alignment of the physiological axes. Malalignment can manifest in the frontal plane as *varus* (bow-legged) or *valgus* (knock knee) deformities (Figure 2.6). Frontal plane alignment plays a role in determining the severity of the progression of OA, and the directions varus or valgus determines which compartment (medial or lateral) of the knee joint is affected [79].

Valgus malalignment shifts the mechanical axis laterally, increasing the load on the lateral compartment of the knee. The lateral shift in the mechanical axis causes excessive stress on the lateral compartment, accelerating cartilage degeneration and contributing to the progression of lateral compartment OA [78, 79]. *Varus malalignment* occurs when the mechanical axis deviates medially, and is typically associated with medial compartment OA [56, 78]. The shift in the mechanical axis results in disproportionate stress on the medial side, accelerating the wear and tear of the articular cartilage and leading to a rapid progression of medial compartment OA. Research has demonstrated that varus alignment results in a higher load on the medial compartment of the knee [58]. The impact of valgus alignment on load distribution may not be comparable to that of varus alignment. In a

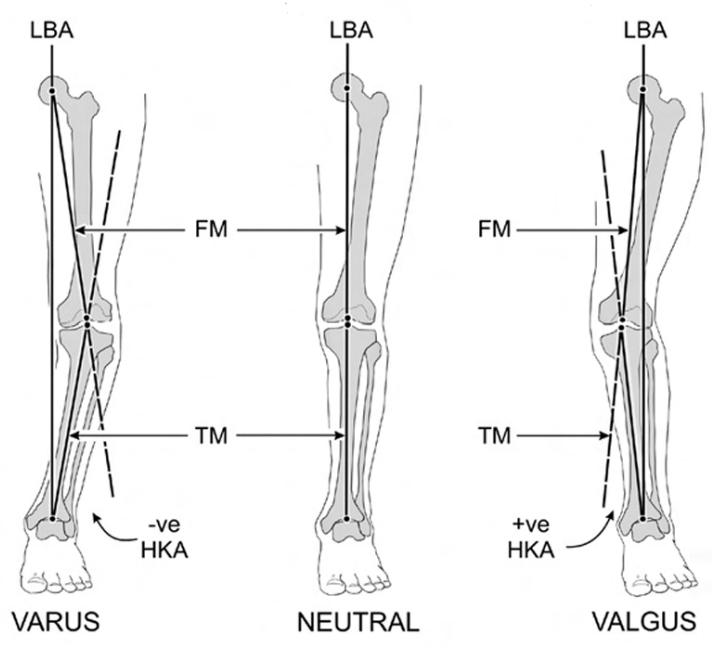


Figure 2.6: Lower Limb Alignment
(Adapted from [88])

normally aligned, ambulating knee, the load is disproportionately transmitted to the medial compartment [80]. This means that even in the absence of any malalignment, the medial side of the knee experiences more load. Varus alignment would have a stronger effect on the risk of medial compartment progression compared to the effect of valgus alignment on the risk of lateral compartment progression. A study by Hsu et al [36] showed that when simulating a one-legged weight-bearing stance by shifting the upper-body gravity closer to the knee joint, 75% of the knee joint load passed through the medial tibial plateau. Therefore, it is reasonable to assume that medial compartment OA occurs more frequently than lateral compartment OA due to mechanical loading. The incidence of varus or valgus malalignment may impair joint repair and maintenance, indicating a need to design and evaluate interventions that alter the knee's loading pattern.

2.2.2 Clinical Interventions

Currently, there is no cure for OA, and treatment options are aimed at symptom management, which depends on the severity of OA in addition to radiological evidence. Various

criteria have been established to determine the severity of OA based on radiological assessment. For example, Kellgren and Lawrence [41] developed a widely used five-point rating scale (0 – No OA, 4 – Severe OA) based on radiographic assessment of joint space width, the presence or absence of osteophytes, and subchondral bone sclerosis. Altman et al. [5] outlined criteria for diagnosing knee OA, which include knee pain and at least one of the following: age over 50 years, morning stiffness lasting no longer than 30 minutes, or crepitus (cracking or popping sounds or sensations) during active motion. Depending on the severity, treatment options can be categorized into surgical and non-surgical interventions. Non-surgical techniques include physical therapy, weight reduction, non-steroidal anti-inflammatory drugs, intra-articular injections, and bracing [24, 82]. Non-surgical options have shown to be effective but pose some limitations in treating severe cases of OA and are best when used in conjunction.

Surgical treatment options for OA are considered when conservative measures fail to provide sufficient relief from symptoms. Primary surgical options include arthroscopic lavage and debridement, cartilage repair techniques, osteotomies, and partial or total knee arthroplasty [74, 82]. The choice of surgery is individualized taking into account the patient's unique clinical scenario, overall health, activity level, and the severity of the OA.

2.3 High Tibial Osteotomy

For knees affected by medial compartment OA, *Opening Wedge High Tibial Osteotomy* (HTO) is an effective surgical intervention for interrupting disease progression [22, 64, 83]. HTO is performed by making an angulated cut in the tibia and creating a wedge that realigns the joint and shifts the load-bearing axis towards the lateral compartment, effectively unloading the affected medial compartment [64, 76]. HTO is a joint-preserving surgery that extends the life of the native knee and often delays, or avoids, the need for a partial (PKA) or total knee arthroplasty (TKA). The surgery is typically performed on young-active patients under 60 years of age with unicompartmental OA who require high knee function and wish to postpone the need for a total knee replacement.

2.3.1 Surgical Technique

Precise preoperative planning is one of the most important steps in HTO. Patient selection and radiological assessment of OA are crucial for preoperative planning [13]. Detailed imaging, including weight-bearing X-ray, MRI, or CT scan, is essential to assess the extent

of OA, bone quality, and knee alignment. Preoperative planning for HTO is typically performed on an anteroposterior long-leg view radiograph [52] using several methods [21, 26, 55], in conjunction with software like PACS to determine the optimal realignment. Radiographic limb alignment analysis is first done to determine the load-bearing axis by drawing a line from the center of the hip to the center of the ankle. The crossing point of the load-bearing axis at the tibial plateau is expressed as a percentage of the total length of the tibial plateau, with 0 % at the most medial edge and 100 % at the lateral edge [52] (Figure 2.7). The magnitude of the correction is typically aimed at shifting the weight-bearing axis from the medial to the lateral compartment, ideally passing through the Fujisawa point (Figure 2.7), which is about 62.5 % of the tibial plateau from medial to lateral [31]. An axis is drawn from the hip joint center to the ankle level, passing through the Fujisawa point to mark the optimal load-bearing axis. Another line is drawn to the hinge point, and a line of the same length is extended to reach the optimal load-bearing axis. For OWHTO, the lateral cortex of the tibia, adjacent to the tip of the fibular head, is chosen as the hinge point. The angle formed by these two lines is measured as the optimal correction angle, as suggested by Miniaci et al [55].

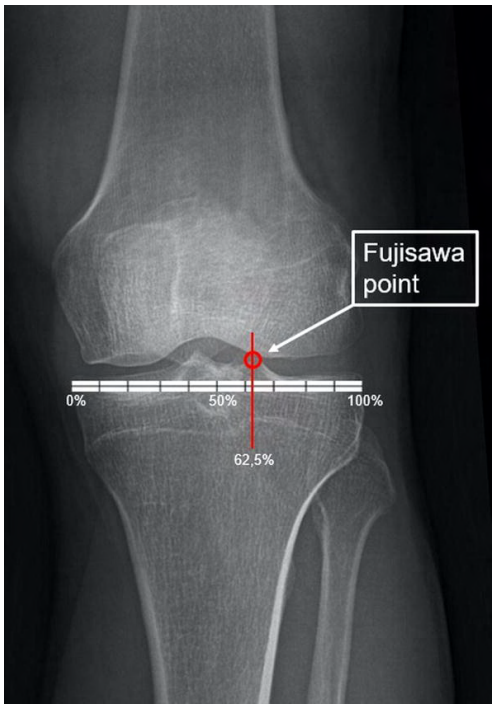


Figure 2.7: Fujisawa point
(Adapted from [66])

The patient is positioned supine on a radiolucent operating table. The surgery is typically performed under fluoroscopic guidance. A 5-cm vertical incision is made between the medial tibial tuberosity and the posteromedial tibia below the joint line. Two guide wires are inserted 3.5-4 cm below the medial joint line towards the fibular head, confirmed by fluoroscopy. A tibial osteotomy is performed below the guide wires with an oscillating saw, extending from the tibial tuberosity to 1 cm medial to the lateral tibial cortex. The osteotomy is opened with a valgus force, and a calibrated wedge is inserted to the desired extent. Once the correction is verified with fluoroscopy, internal fixation is achieved using a metal plate, and the defect is grafted with appropriate bone graft materials [28, 43] (Figure 2.8).



Figure 2.8: Opening Wedge High Tibial Osteotomy. A) A guide wire is placed 3.5-4 cm below the medial joint line to about 1 cm below the lateral articular margin of the tibia B) Osteotomy performed with an oscillating saw C) Medial tibia opened with a wedge (Adapted from [43])

2.3.2 Clinical Outcomes

Osteotomies are usually performed in mid-aged patients under 60 years who engage in high-demand activities and delay the need for a knee replacement. Short and long-term outcomes of HTO are typically assessed through a follow-up evaluation system targeting survivorship, return to sport, and patient-reported outcomes. Failure of the procedure is defined as conversion to arthroplasty or revision HTO [38]. Treatments have shown successful short-term survivorship, but long-term outcomes deteriorate with time. A summary of survivorship of HTO reported in current literature is provided in Table 2.1.

Table 2.1: Studies reporting survivorship of HTO

Study	Year	Survival rate			
		5 years	10 years	15 years	20 years
Coventry et al [23]	1993	90%	65%	-	-
Naudie et al [61]	1999	73%	51%	39%	30%
Billings et al [9]	2000	85%	53%	-	-
Koshino et al [42]	2004	97.8%	96.2%	93.2%	-
Fletcher et al [27]	2006	94.8%	92.8%	89.7%	85.1%
Azukuzi et al [4]	2008	97.6%	90.4%	-	-
Hiu et al [38]	2010	95%	79%	56%	-
Niinimäki et al [62]	2012	89%	73%	-	-
Polat et al [70]	2017	93.4%	71.2%	-	-
van Wulfften Palthe et al [87]	2018	-	75%	55%	40%
Song et al [81]	2019	100%	91%	63.4%	48.3%
Constantin et al [18]	2024	85%	77%	63%	44%

The long-term success of HTO declines over time, with some studies reporting failures that required revision HTO or arthroplasty for patients. The study by Billings et al [9] reported that twenty-one out of the sixty-four knees that underwent HTO were treated with a subsequent TKA. Fletcher et al [27] reported survival rates of 313 knees and forty-three knees (14%) underwent knee arthroplasty at an average of 8.5 years post-surgery. Hiu et al [38] reported that 84% would undergo revision HTO at a mean of 12 years of follow-up. Polat et al [70] reported 16% of the patients studied required TKA at a mean of 8.9 years after HTO.

Factors affecting success of HTO

Several factors can impact the long-term success and failure of HTO, including native and post-surgical biomechanical factors. The biomechanical environment of the knee joint post-surgery is crucial for the long-term viability of the procedure. Among the various complications associated with HTO, the most common include loss of correction, fractures of the lateral cortex and articular cartilage, joint-line obliquity, implant failure, inadvertent increases in the tibial slope leading to abnormal pressure distributions, MCL strain, under-correction or over-correction, and neurovascular injuries [30, 53, 63]. Many such complications can be mitigated through adequate patient selection and preoperative planning procedures. There is ongoing debate about the ideal candidates for HTO and the appropriate degree of correction. While patients with severe bony deformities are clear candidates, many fall into a gray area with milder deformities. Another debated issue is how best to shift the load-bearing axis, i.e., if the correction be made to the tibia alone, the femur alone (distal femoral osteotomy) [85], or through a double osteotomy of both the tibia and femur to maintain joint line obliquity [7]. In addition, intraoperative decisions can influence the success of the osteotomy. These include the placement and trajectory of the cortical hinge, hardware selection, soft tissue involvement, and the use of grafts to fill osteotomy gaps. The effectiveness of these factors continues to be debated.

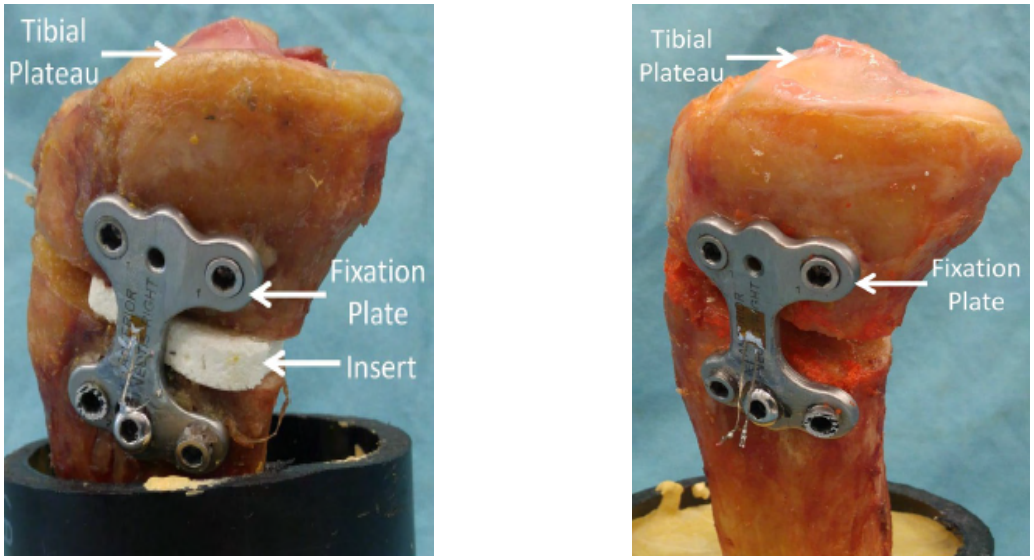
Among the preoperative planning factors, determining the optimal correction angle is among the most critical for the long-term clinical success of HTO. Yet, deciding on the optimal angle has been a source of much debate. Failing to target the ideal alignment can lead to poor outcomes, such as progressive OA, failure of HTO, and patient dissatisfaction. Literature also suggests that the MCL becomes strained during osteotomy opening and may create abnormal pressure distributions across the tibia plateau [86]. The MCL is a critical stabilizing structure within the knee joint, and any disruption to its normal function could have significant implications for the joint's load-bearing characteristics. However, it is unclear what specific parameters of the osteotomy influence this strain, and the implications of additional or residual strain within the MCL on pressure distribution. The subsequent sections provide an overview of past and current biomechanical studies on the HTO procedure.

2.4 Experimental Studies

In-vitro mechanical testing methods have been conducted to assess and evaluate HTO and the biomechanical factors associated with it. In-vitro studies typically involve test-

ing on cadaveric specimens to quantify knee joint mechanics including correction angle optimization, tibiofemoral pressure distributions, and MCL strain.

A study by MacDonald et al [50] evaluated the effectiveness of a synthetic bone insert and a fixation plate in improving the integrity of opening wedge HTO and reducing tensile strains in response to post-surgical loading. Twelve knee specimens were used, in which six knees had a synthetic bio-absorbable wedge and were secured with fixation plates (Figure 2.9a), and the remaining six knees were secured only with a fixation plate (Figure 2.9b). The knee specimens were subjected to a cyclical loading between 100N and 800N until failure. Peak strains were found in the fixation plates and compared in both conditions. The study found that the inclusion of the wedge insert had a significant impact on the strain patterns observed on the fixation plate and lateral cortex during the HTO procedure. With the wedge insert, the fixation plate experienced compressive strains, whereas without the wedge, the plate transitioned to tensile strains. The strains measured at the lateral cortex were significantly impacted by the inclusion of an insert, increasing from a compressive strain of -55.6 to 23.7 when only the plate was used. The author concluded that the addition of a synthetic insert limited the tensile strains at the plate and lateral cortex, suggesting that the wedge insert plays an important role in load distribution and protection around the osteotomy site.



(a) (b)

Figure 2.9: (a) Synthetic insert with fixation plate (b) Fixation plate only (Adapted from [50])

Mina et al [54] investigated the correlation between correction angles and knee joint loading patterns using electronic pressure sensors in cadaveric knee specimens. Eight cadaveric specimens underwent testing with 10 different adduction angles using an osteotomy spreader to mimic HTO treatment. Force, contact area, and pressure distribution were recorded at each alignment. The study showed that as the tibiofemoral alignment was shifted, the medial compartment contact pressure and contact area decreased and were shifted to the lateral compartment. They recommended a valgus alignment of 0°– 4° for optimal stress distribution between the medial and lateral compartments, regardless of condylar width, baseline tibiofemoral alignment, body weight, or chondral defect size.

Effect of MCL release on Cartilage pressures

Agneskirchner et al [2] evaluated the effects of a valgus open wedge high tibial osteotomy on the articular cartilage pressure distributions on six human knee cadavers. The knee specimens were tested with a load of 1000N in a material testing machine using a specially designed fixture (Figure 2.10) while simulating different loading alignments (varus, straight, and valgus). Articular cartilage pressures were measured using pressure-sensitive films in the medial and lateral compartments. The study had two major aspects. The first aspect of the study had measurements performed with an intact MCL. The second aspect of the study had measurements performed while gradually dissecting the MCL (50% release and 100% release).

The study found a significant correlation between the load distribution and the position of the loading axis, with the medial compartment predominantly loaded in the varus setting. The opening wedge HTO without MCL release resulted in a significant increase of pressure medially, while only after complete release of the MCL was a significant decrease of pressure medially observed.

Egmond et al [86] investigated the impact of a medial open wedge HTO and the release of the superficial MCL on tibiofemoral cartilage pressure, MCL tension, and valgus laxity in human cadaveric knees. Seven fresh-frozen knees were used, with medial and lateral mean contact pressure, peak contact pressure, and contact area measured using a pressure-sensitive film, and MCL tension measured with a custom device. Measurements were recorded for a 10° correction over 5 minutes and 24 hours for one knee. The superficial MCL was then released, and the same measurements were taken. Following a 10° OWO, MCL tension decreased by 10.7% in 5 minutes and by 24.2% in 24 hours. After the osteotomy, medial compartment mean contact pressure, peak contact pressure, and contact area increased, while lateral compartment values decreased. After releasing the superficial MCL, the medial compartment mean contact pressure, peak contact pressure, and contact

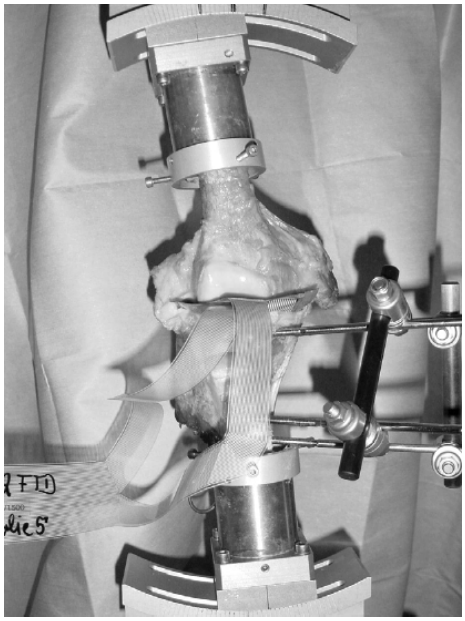


Figure 2.10: Cadaveric knee specimen, mounted into the testing fixture (Adapted from [2])

area decreased, while lateral compartment values increased. Additionally, valgus laxity increased by a mean of 7.9°. The study concluded that releasing the superficial MCL helps reduce medial cartilage pressure following an osteotomy but significantly increases valgus laxity, potentially impacting knee stability.

Pape et al [65] aimed to evaluate the effect of partial and complete release of the superficial MCL during open wedge HTO on medial joint opening under valgus stress. The article hypothesized that partial MCL release would not significantly impact valgus stability. A cadaveric study of 10 knee specimens was performed where the superficial and deep MCL were sectioned and the medial joint opening was measured with a standardized valgus load. The results showed no significant differences in medial joint opening between complete and partial release of the superficial MCL. The authors concluded that the anterior fibers of the superficial MCL play an important role in maintaining valgus stability, and therefore the release of the superficial MCL during open-wedge HTO should be minimized, especially in patients with small wedge sizes and pre-existing laxity, to reduce the risk of late valgus instability.

2.5 Finite Element Studies of HTO

The complexities associated with knee osteotomies are owed to their multi-factorial nature, making it difficult to research using traditional clinical methods and in vitro testing. While in vitro mechanical testing offers some insights into the pressure and load distribution at the knee joint, it has limitations that hinder detailed quantitative investigation into knee joint mechanics. Computational approaches, like finite element (FE) models, can be an effective biomechanical tool to plan surgical procedures and predict patient-specific outcomes. Development of three-dimensional (3D) FE models of biological systems is typically performed through CT or MRI techniques that can precisely capture patient-specific geometries [83]. FE models of the knee joint can provide valuable insights into several crucial factors in the pathogenesis of OA such as contact forces and stresses in the joint, ligament mechanics and injury, geometric and material behavior of articular cartilage and menisci, and patient-specific post-surgical outcomes. The subsequent sections provide an overview of existing literature on knee joints and HTO-specific FE models.

2.5.1 FE studies of HTO procedure

Articular cartilage contact pressure studies

Trad et al [84] carried out 3D FE analyses to investigate the effects of varying correction angles on stress distribution in the knee joint. The analyses were performed by varying the correction angles from 0° to 10° valgus. The developed models were validated against experimental and numerical results. The study found that an increase in correction angles shifted the loading from the medial to the lateral compartment. The Von Mises and shear stresses decreased in the medial compartment and increased in the lateral compartment. A balanced distribution of stresses between the two compartments was noticed at 4.5° correction.

In a study by Zhang et al [93], 3D FE models of the knee joint were developed from MRI images to simulate medial open wedge HTO to determine the compressive and shear stress distributions on the articular cartilage for varying correction angles. Corrections were varied from 2.5° valgus to 10° degree valgus with an increment of 2.5°. The results showed the peak compressive and peak shear stresses in the medial compartment decreased as the loading axis shifted laterally but the lateral compartment increased the peak stresses. The FE analysis also demonstrated that a correction of 7.5° effectively reduced the loads in the medial compartment and achieved a more ideal situation with stresses most uniformly distributed between these two compartments.

Nakayama et al [60] analyzed the resultant stress induced by joint-line obliquity after HTO for varus knee deformity using a 3D FE model analysis. Axial loads of 1200 N were applied on models with corrections of 2.5°, 5°, 7.5°, and 10° simulated to the mechanical environment of a knee with obliquity. The results showed a significant increase in shear stress in the medial compartment at obliquity angles of 5° or more, with stress values rising from 1.6 MPa (normal knee) to 7.2 MPa at 10° obliquity. The study concluded that joint-line obliquity greater than 5° results in excessive shear stress in the tibial cartilage, suggesting that double-level osteotomy should be considered to avoid detrimental stress in cases of significant correction.

2.6 Summary

The studies reviewed offer significant insights into the impact of high tibial osteotomy HTO on knee joint contact parameters. Studies have shown that FE models can be an effective biomechanical tool to predict contact behaviors of soft tissues after an HTO procedure. However, several gaps and limitations have been identified. Investigations into the strain in the medial collateral ligament (MCL) post-surgery and its effects on knee joint contact parameters are yet to be addressed computationally. Additionally, the feasibility of MCL release to reduce joint contact pressures has not been explored computationally. Current FE models in the literature often do not include the hip and ankle joints, which are essential for determining the optimal correction for an HTO procedure. In addition, the presence of hip and ankle joints in the models offers a more accurate representation of lower limb mechanics by providing appropriate boundary conditions. Furthermore, the efficacy of a double osteotomy procedure for larger corrections has not been addressed computationally in the literature. Addressing these gaps would enhance the understanding and application of HTO in clinical practice.

2.7 Hypothesis

The hypotheses for the current research are as follows:

1. The contact and load distribution in the medial compartment of the knee will decrease following HTO and increase in the lateral compartment, thereby reducing the stress on the medial cartilage.

2. Larger corrections achieved through HTO will result in increased strains in the MCL that will subsequently overload the medial compartment.

3. By releasing the MCL, the pressure distribution on the medial compartment will be reduced.

4. Implementing a double osteotomy for cases requiring large corrections will produce a more even distribution of loading across the knee joint.

Chapter 3

Methodology

The methodology of the current study can be broken into four major phases. Figure 3.1 shows an overview of the steps involved in the development of the FE model.

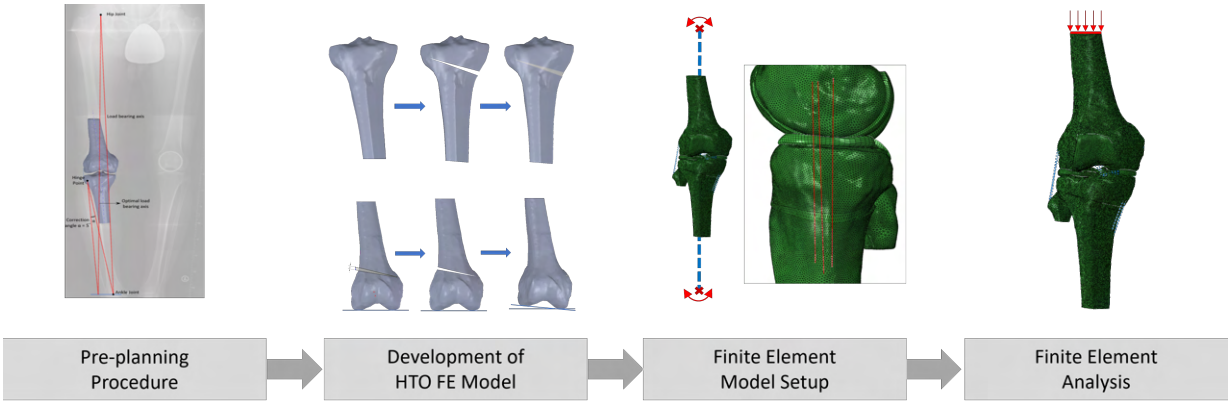


Figure 3.1: Overview of steps involved in the development of FE model

3.1 Development of Finite Element Model

3.1.1 Finite Element Knee Model Origin

The FE model to simulate different osteotomy corrections was built using an existing 3D model of the knee joint developed by Rao [71]. The modeling process adopted by Rao

began with obtaining CT and MRI images of a knee joint cadaver of a 50th-percentile male. The images when stacked on each other in sagittal, frontal, and transverse planes produced a solid geometry of the knee. 3D geometries of the bones, cartilages, and menisci were identified and extracted with a combination of automatic and manual segmentation processes in an open source software called *3D slicer*, as shown in Figure 3.2. The extracted geometries were then imported to SolidWorks for further smoothing and post-processing.

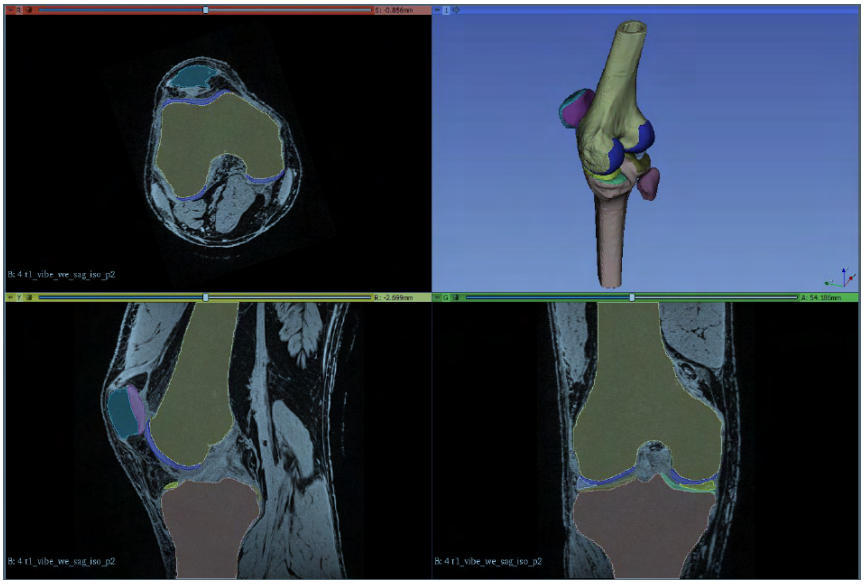


Figure 3.2: Knee segmentation from MRI scans on 3D Slicer
(Adapted from [71])

Attachment sites of the ligaments were identified and marked on the cadaver to digitize anatomical landmarks in the knee. The internal surfaces of the knee joint were first exposed by cutting through the mid-lengths of the cruciate and collateral ligaments. Bony landmarks were identified and referenced as the ligament attachment sites. A coordinate measuring device, *MicroScribe-G2XTM* (Immersion Corporation, USA), was used to record the locations of the ACL, PCL, MCL, and LCL attachment sites relative to these bony landmarks. The coordinates of these locations were then matched to the 3D model in 3D Slicer and later imported into *Abaqus CAE 2022* (Dassault Systèmes, Johnston, RI), the selected FE software package for the study. An overview of this process is provided in Figure 3.3.

Ligaments were modeled using Abaqus' non-linear axial connector elements by inputting force versus displacement curves. The pre-strain in each ligament bundle was

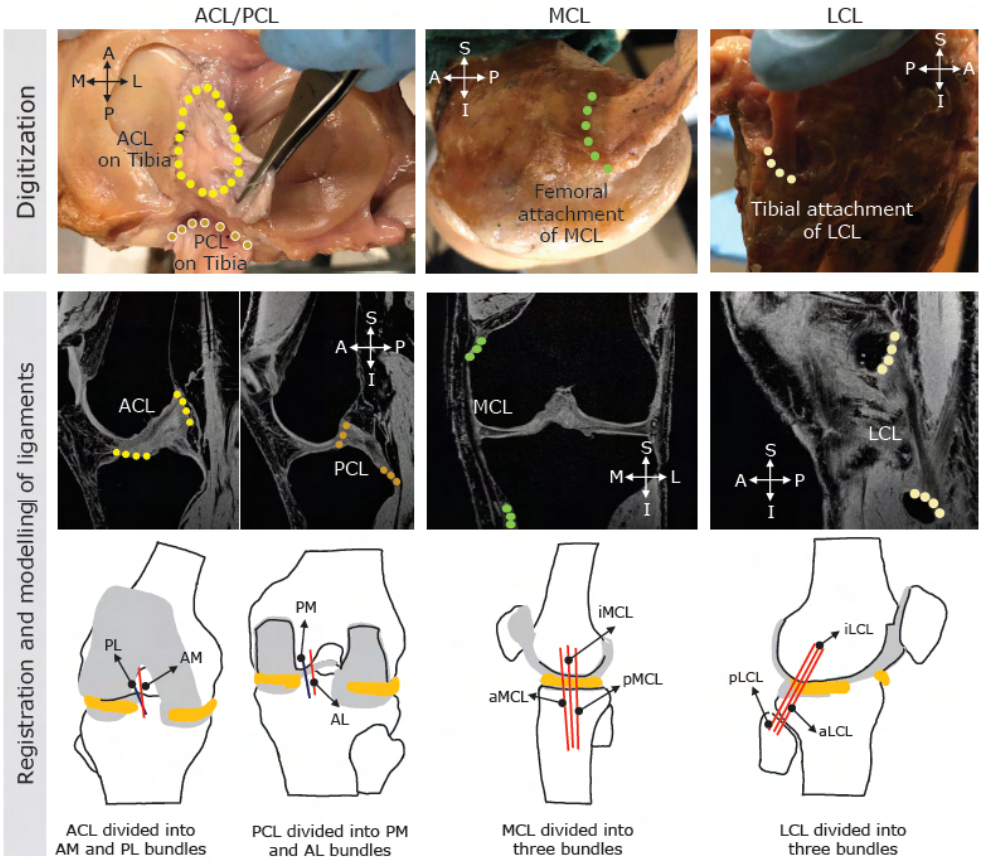


Figure 3.3: Digitization process of ligament insertion
(Adapted from [71])

specified through their respective zero-load lengths, L_0. Stiffness values for all ligaments, except for the ACL, were obtained from Blankevoort et al [10, 11]. The ACL stiffness parameters were derived from Chandrashekar et al [17] and modeled as two parallel nonlinear springs representing the anteromedial (AMACL) and posterolateral (PLACL) bundles. Only the superficial MCL was modeled in the current study, the deep MCL was ignored. A list of stiffnesses of the major ligaments is given in Table 3.1. In addition to the major ligaments of the knee joint, meniscal ligaments were defined to secure the ends of the menisci to the tibial plateau. The ligaments were defined at the anterior and posterior ends of both the lateral and medial menisci as linear springs with a stiffness of 180 N/mm each [34]. A small rigid body was connected to the ends of the menisci using TIE constraints to prevent instabilities that could arise from stretching a single node.

Table 3.1: Ligament bundles used in the FE model (Adapted from [72])

Ligament	Ligament Bundle	Stiffness Parameter, k	Strain at extension, ϵ	Referenced Study
ACL	Anteromedial	NA	0.06	Chandrashekar et al [17]
	Posterolateral		0.10	Blankevoort et al [11]
PCL	Posteromedial	9000	-0.15	Blankevoort et al [10]
	Anterolateral	9000	-0.03	
Superficial MCL	Anterior	2750	0.04	Blankevoort et al [11]
	Intermediate	2750	0.04	
	Posterior	2750	0.03	
LCL	Anterior	2000	-0.25	Blankevoort et al [11]
	Intermediate	2000	-0.05	
	Posterior	2000	0.08	

Bones were modeled with stiffer material properties and were meshed using tetrahedral elements in Hypermesh, then assigned as rigid bodies in the FE model. The meniscus and cartilage, being softer tissues with lower material stiffness, were modeled using hexahedral mesh elements in IA-FEMesh. These meshed geometries were subsequently imported into Abaqus and assembled. The cartilage was constrained to their respective bones using TIE constraints, ensuring no relative motion between them. A frictionless contact was defined between the cartilage and meniscus to allow smooth sliding. The material property data for bones and soft tissues are shown in Table 3.2.

Table 3.2: Material property data for bones and soft tissues

Model component	Young's Modulus	Poisson's Ratio	Referenced Study
Bone and Graft	8 GPa	0.3	[25]
Cartilage	20 MPa	0.45	[3]
Menisci	59 MPa	0.49	[44]

3.1.2 Pre-planning procedure

To accurately simulate the pre and post-surgical environments of HTO, the model developed by Rao [71] was further modified to meet the objectives of the current study. The development of a FE model emulating the surgical procedure required a comprehensive pre-planning procedure. The pre-planning procedure mentioned in Section 2.3.1 was adopted

for the current study, based on Miniaci et al [55]. The procedure is typically done on imaging software like *PACS* on a long-standing anteroposterior (AP) radiograph of the lower limb that includes the hip, knee, and ankle joints to mark the load-bearing axis which is crucial for determining the severity of OA and the optimal correction required. Although the model developed by Rao (Figure 3.4b) accurately represents the anatomy of the knee joint, it does not include the hip and ankle joints since the cadaver specimen (Figure 3.4a) contained only the knee joint.



(a) (b)

Figure 3.4: (a) Cadaver specimen (Adapted from [72]) (b) 3D model of the knee joint

Further steps were taken to address this limitation since accuracy in determining the optimal correction is one of the most crucial steps in the HTO procedure. To accurately plan the surgical procedure, a long-standing radiograph of the lower limb that best fits the model was necessary to determine the optimal correction angle. A long-standing radiograph in Lu'ıs et al [49] was utilized by aligning an image of the model consisting of the tibia and femur onto the radiographic image. Using imaging tools, the load-bearing axis and the joint line were marked on the image to determine whether or not there was a deviation of the axis from the center of the knee joint. As shown in Figure 3.5, the axis did not pass through the center of the knee joint but was rather passing medially to the knee joint, indicating a varus deformity. To address this, the optimal load-bearing axis was marked from the hip joint passing through the Fujisawa point [31] (Figure 2.7). Using the pre-planning procedure by the Miniaci method [55], the degree of varus deformity was

measured and the optimal correction angle was determined to be 5 degrees. The accuracy of this procedure was validated with the help of Dr Sebastian Tomescu, an orthopedic surgeon at Sunnybrook Hospital, Toronto.

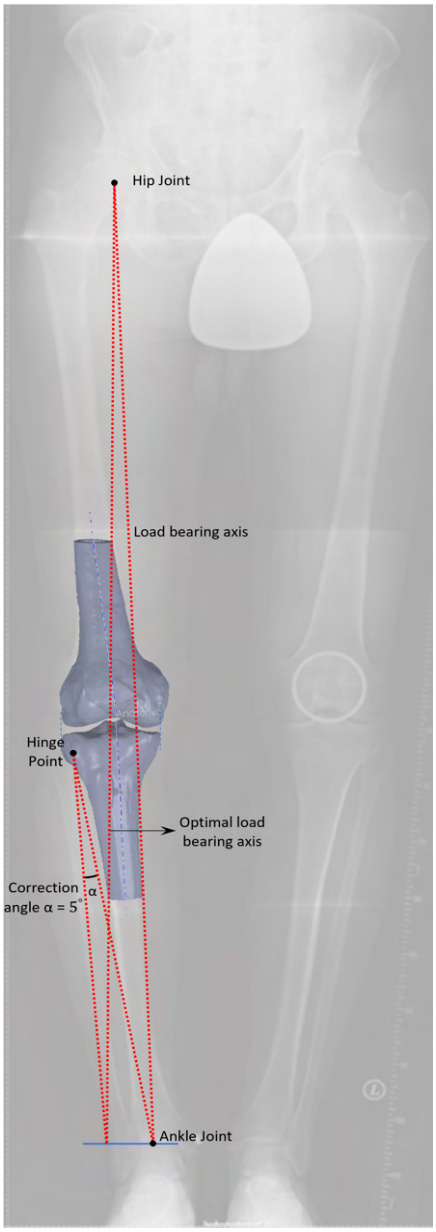


Figure 3.5: Pre-planning procedure for HTO

3.1.3 Surgical Simulation of HTO

Combining the modeling efforts by Rao and the pre-planning procedure, models with different osteotomy correction angles (under-correction, optimal correction, and overcorrection) were constructed using CAD software package *Solidworks* (v2020, Dassault Systemes). This process aimed to simulate the osteotomy cut, remove a bone wedge, and subsequent realignment of the tibia to achieve the desired correction angles.

The modeling process began with opening the pre-existing 3D model of the tibia in *SolidWorks*. The tibia model was split into two distinct parts, as shown in Figure 3.6. This was accomplished by defining a cutting axis that passes through the osteotomy hinge point, starting from the site where the osteotomy cut is to be made. The site of the osteotomy cut and the hinge point were precisely marked on the model with the help of the orthopedic surgeon. This step is essential for creating a realistic simulation of the osteotomy procedure, as it sets up the tibia for the subsequent realignment.

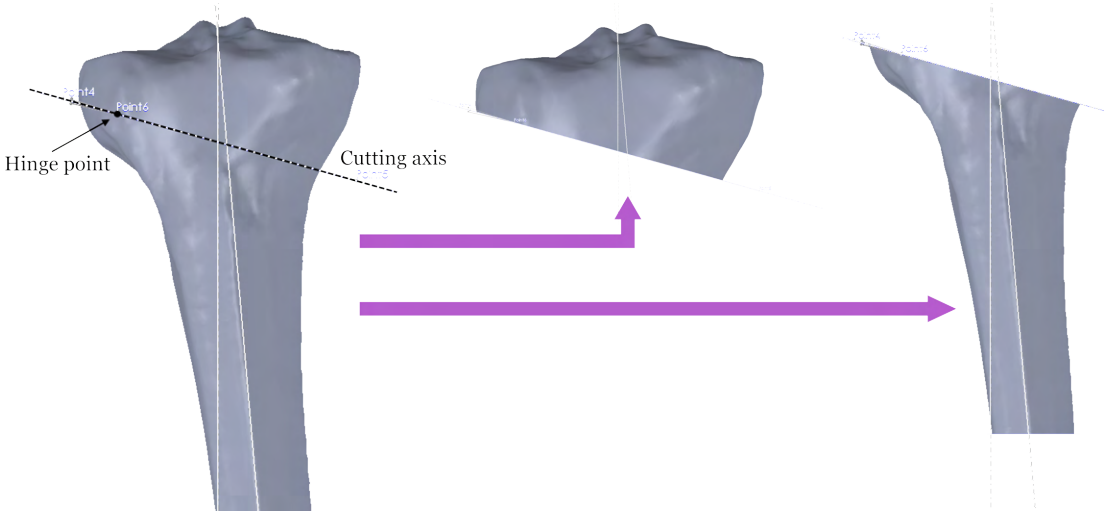


Figure 3.6: Tibia split into two parts by defining cutting axis

The osteotomy cut was simulated by removing a small wedge of bone on the lateral side of the tibia, extending up to the hinge point (Figure 3.7). The removal of the wedge on the lateral side was crucial, as the wedge's angle directly represented the desired correction angle. Removing the wedge exposed two distinct surfaces on the tibia model: one on the upper segment and one on the lower segment. The exposure of these surfaces is a key step in the modeling process, as it allows for the realignment of the tibial segments.

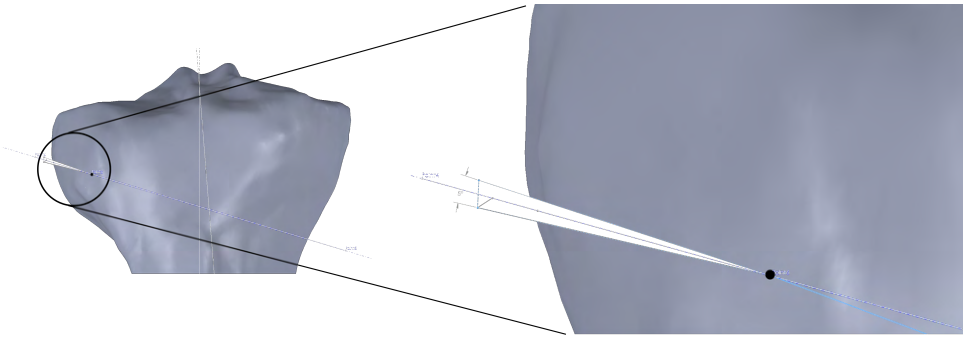


Figure 3.7: Removal of the wedge on the lateral side of the tibia

The next step involved rotating the distal part of the tibia around the osteotomy hinge. This rotation was achieved by mating the two exposed surfaces using *SolidWorks* mating tools. The mating process ensured that the two surfaces aligned correctly, simulating the realignment of the tibia as performed during the surgical procedure. As the tibia segment was rotated, an opening on the medial side of the tibia was created which represents the wedge formed by the opening of the osteotomy cut and the realignment of the tibia in a real surgical scenario. Finally, the osteotomy cut and the resulting opening were filled with a graft to stabilize the tibial segments in their new alignment. An overview of the process for a 5° correction is shown in Figure 3.8.

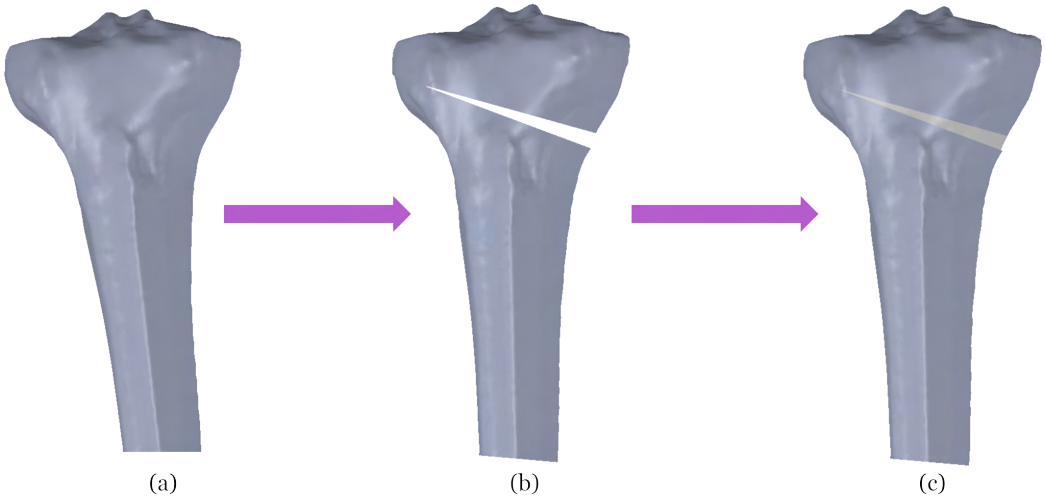


Figure 3.8: (a) Uncorrected tibia model (b) Tibia with an osteotomy wedge cut and opening (c) Wedge filled with graft

The modeling process was conducted for three different correction angles: 4 degrees (under-correction), 5 degrees (optimal correction), and 7 degrees (over-correction). This variation in correction angles allowed for a comprehensive analysis of the impact of different degrees of correction on the articular cartilage contact pressures and MCL strain.

3.1.4 Double Osteotomy model generation

In addition to modeling single-level HTO procedures, the bone geometries for double-level osteotomy procedures were also created. This involved both the tibia and the femur to address more significant deformities that cannot be corrected adequately with a single osteotomy. For the femur, a lateral distal closing wedge osteotomy was performed using the femur model in *SolidWorks*. The lateral distal closing wedge osteotomy on the femur model involved similar steps to those used for the tibial osteotomy. The femur was split into two parts along a defined cutting axis, and a wedge of 3° was removed from the lateral distal part. The distal segment of the femur was then rotated to close the wedge, ensuring the two new surfaces were mated correctly to simulate the realignment. The same modeling procedure was applied to the tibia as described previously and was corrected to 4°.

The overall correction for the double-level osteotomy was considered to be 7°, a typical value for medium to larger deformities that may require the combined effect of corrections in both the tibia and femur [60]. This procedure effectively shifts the load-bearing axis and corrects the deformity by realigning both the tibia and femur. An overview of the process is shown in Figure 3.9.

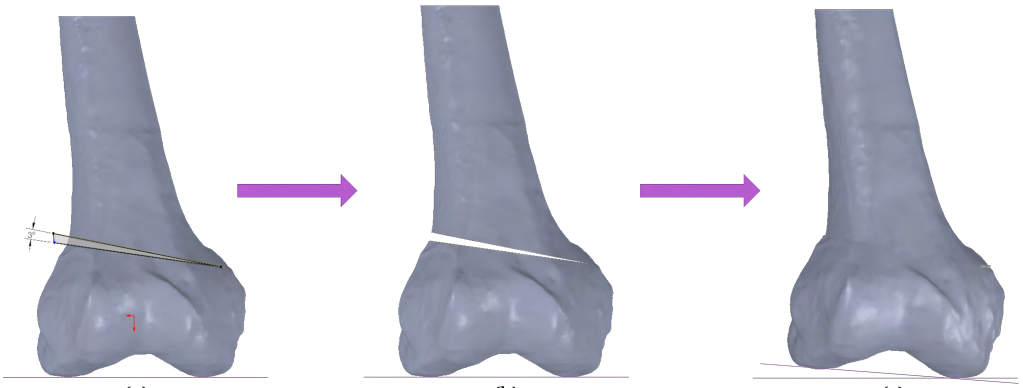
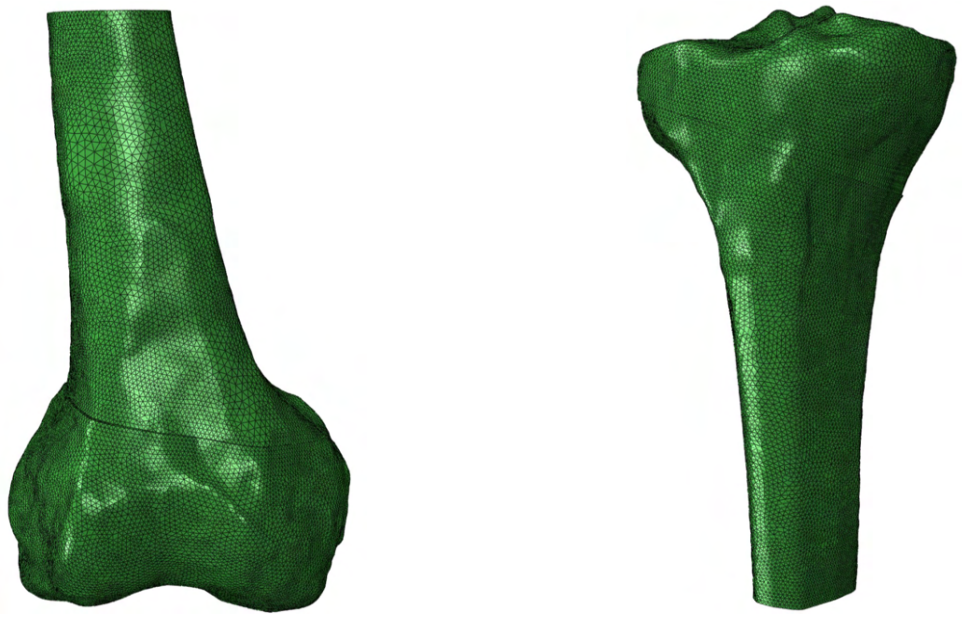


Figure 3.9: (a) Uncorrected femur model marked with correction angle (b) Removal of wedge from the lateral side (c) Wedge closed to simulate distal femoral osteotomy

3.1.5 Meshing of the bones and soft tissues

In the FE model, the knee joint bones (tibia and femur) were treated as rigid bodies due to their relatively higher stiffness compared to soft tissues. This approach is commonly employed in FE studies focusing on soft tissue behavior [25, 45, 67, 69]. Treating the bones as rigid bodies reduces computational time, as the elements within a rigid body do not deform but only display rigid body motions. Therefore, the bones were meshed using first-order tetrahedral elements in *HyperMesh* (Figure 3.10). The meniscus and cartilages were softer tissues with lower material stiffness, hence they were modeled by Rao using hexahedral mesh elements in a software called *IA-FEMesh*. These meshed geometries were then imported to Abaqus and assembled.



(a) Meshed Femur (b) Meshed Tibia

Figure 3.10: Tetrahedral meshes of the bones

3.2 Finite Element Analysis

The individual meshes of the bones were imported and assembled with the soft tissues in *Abaqus CAE*. Appropriate material properties were assigned to the assembly components. Contacts and constraints were defined to accurately emulate the interactions between the components, based on [71]. The following section explains in detail the steps involved in the analyses for various conditions to meet the specific objectives.

3.2.1 Loading and Boundary conditions

To simulate realistic physiological conditions, a distributed load equivalent to 800N was chosen and applied to the proximal surface of the femur in each model. The 800N load was gradually applied using a ramp magnitude, ensuring a realistic application of force. This represents the typical force exerted during weight-bearing activities, providing a relevant stress scenario for the knee joint. Nonlinear static analyses were carried out to capture the contact behavior of soft tissues under loading. The loading application is shown in Figure 3.11.

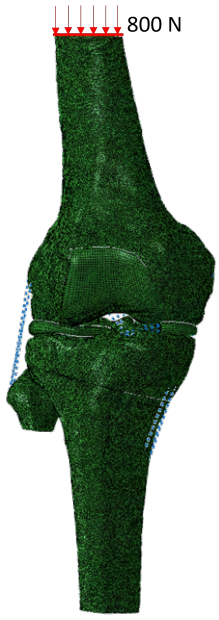
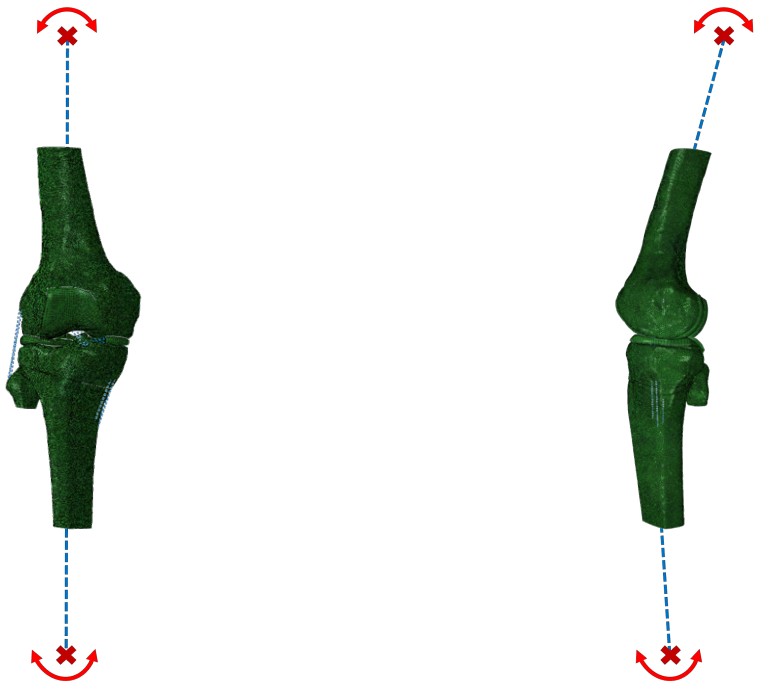


Figure 3.11: Distributed load of 800N on femur

The boundary conditions were established at the reference points of the hip and ankle joints, allowing for motion in the frontal and sagittal planes while constraining axial rotation, based on the methodology described by Agneskirchner [2]. This approach differs from existing knee FE studies that typically fix the distal end of the tibia and apply a force on the femur without considering the hip and ankle joints. The position of the ankle joints was varied for each model based on the rotation of the tibia after correction. By incorporating these additional boundary conditions, the model offers a more comprehensive representation of the biomechanical environment of the knee joint and the lower limb, and the effect of shifting the loading axes after corrections. This distinction is critical as existing literature often overlooks the contributions of the hip and ankle joints, potentially limiting the accuracy of simulations. Through this approach, the current analysis provides deeper insights into the biomechanical impacts of various HTO procedures, ultimately informing better clinical decision-making. The boundary conditions applied at the hip and ankle joints are shown in Figure 3.12.



(a) (b)

Figure 3.12: Frontal and Sagittal plane motion allowed at hip and ankle joints based on Agneskirchner et al [2]

3.2.2 Validation of FE model

To validate the FE model, a non-linear static simulation was performed by applying an 800N distributed load on the proximal surface of the femur on an uncorrected model. This load mimics the typical axial load experienced by the knee joint during activities such as standing or walking. In line with most contact studies on knee joints, the focus was on the pressure distribution at the articular surface under pure axial loading conditions. Boundary conditions were provided at the hip and ankle joints, as mentioned in 3.2.1.

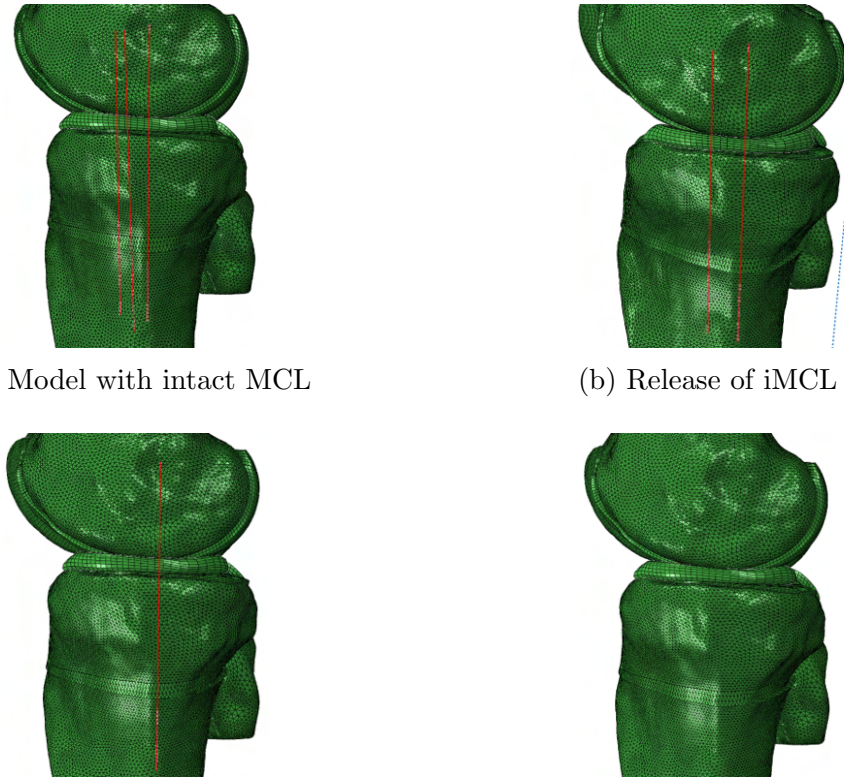
Articular cartilage properties can vary significantly, impacting the simulation outcomes [46]. For validation, two different moduli of elasticity for the articular cartilage were considered for validation purposes: 5 MPa [68] and 20 MPa [3]. The stress and pressure distributions across the articular surface were examined for both cartilage conditions. The simulation results for each modulus of elasticity were then compared with findings from existing literature to validate the model.

3.2.3 MCL Release

Another objective of this study was to investigate the effects of the release of the superficial MCL to evaluate its viability as a surgical technique for reducing medial contact forces and pressures. The release procedure was performed on a model that had been corrected by 5°.

The process for releasing the superficial MCL involved specific adjustments within the finite element model. The superficial MCL was represented using linear spring elements with defined stiffnesses, organized into three distinct springs positioned anteriorly (aMCL), intermedially (iMCL), and posteriorly (pMCL). The release sequence began with the intermediate MCL, followed by the anterior and posterior MCLs. This order was chosen arbitrarily to facilitate a stepwise release.

This stepwise approach allowed for a systematic comparison of the impact on the articular surface, as the release of each component of the MCL could be evaluated independently. The aim was to understand how releasing different parts of the MCL affected the distribution of forces and pressures across the knee joint. By doing so, the study sought to determine whether this surgical technique could effectively reduce medial contact forces and alleviate pressure, potentially offering a viable intervention for patients requiring medial compartment unloading. The process of partial and total release of MCL is shown in Figure 3.13.



(a) Model with intact MCL

(b) Release of iMCL

(c) Release of iMCL and aMCL

(d) Complete release of MCL

Figure 3.13: Partial and total release of Superficial MCL

Similar loading and boundary conditions were applied to the models with released MCL. The results obtained were compared with the results of the model with intact MCL, evaluating key contact parameters, and providing a comprehensive understanding of the changes in knee joint mechanics due to the release of the MCL.

3.3 Contact Outputs and Summary

For all the FE models generated, detailed analyses were performed to evaluate the contact forces (CF), contact pressures (CP), and von Mises stress (VMS) distributions across the articular surfaces of the knee joint. These parameters were crucial in understanding the biomechanical behavior of the knee joint under specific loading and boundary conditions, particularly in the context of the HTO procedure. The contact forces were determined at

the interfaces between the femoral cartilage and both tibial cartilages, as well as between the femoral cartilage and the menisci. This was accomplished by defining contact pairs in Abaqus CAE, specifically: femoral cartilage with medial tibial cartilage (FC-MTC), femoral cartilage with lateral tibial cartilage (FC-LTC), femoral cartilage with medial meniscus (FC-MM), and femoral cartilage with lateral meniscus (FC-LM). The results from these simulations were compared against each other to identify variations and similarities in response among the different correction models, namely uncorrected, under-correction, optimal correction, overcorrection, and double osteotomy. Additionally, the findings were validated against existing literature to ensure their accuracy.

A key focus of this study was the strain experienced by the MCL, as it plays a vital role in knee stability and function. The strain in the MCL was determined by quantifying the total force within the spring elements that represented the ligament in the FE models. This approach allowed for an accurate representation of the MCL's mechanical response under different simulated surgical corrections. By analyzing the MCL strain, the study aimed to provide insights into the implications of various osteotomy corrections on ligament behavior, and the effects on force and pressure distribution across the articular surface. A summary of all the models developed and the outputs generated is shown in Table 3.3.

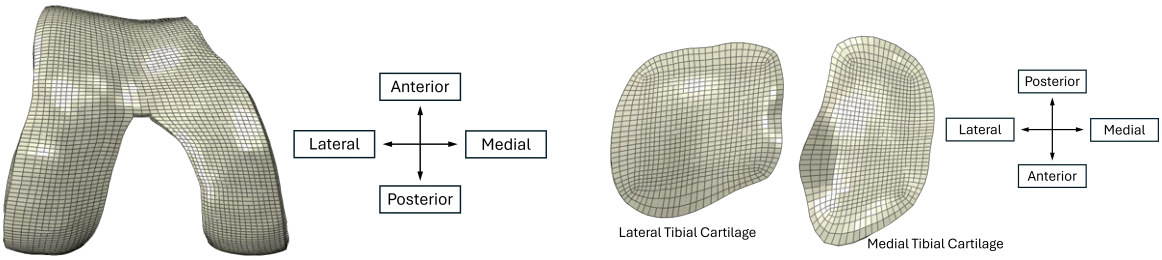
Table 3.3: Summary of FE models developed

FE Models	Outputs generated				
	CF	CP	VMS	MCL Strain	MCL Release
Uncorrected (0°)	✓	✓	✓	✓	-
Under-correction (4°)	✓	✓	✓	✓	-
Optimal Correction (5°)	✓	✓	✓	✓	✓
Overcorrection (7°)	✓	✓	✓	✓	-
Double Osteotomy (7°)	✓	✓	✓	-	-

Chapter 4

Results

This chapter presents the results of all FE analyses conducted in this study. The chapter begins by assessing the mesh quality of the tibia models and the femur model used in double osteotomy. This is followed by detailed results of the cartilage and meniscus contact outputs and the MCL strain outputs, with a comparative analysis between the uncorrected model and various HTO corrections. The contour plots for contact parameters and stress distribution on the femoral cartilage and tibial cartilage are reported. The orientations of the contour plots are shown in Figure 4.1. Furthermore, the outcomes of partial and total release of the superficial MCL are examined, comparing them with the intact MCL condition. Finally, the results of double osteotomy are compared with the results of the overcorrected model. The chapter provides a quantitative analysis of all the simulations run, setting the premise for Chapter 5.



(a) (b)

Figure 4.1: Orientation of Contour plots (a) Orientation of femoral cartilage (b) Orientation of medial and lateral tibial cartilages

4.1 Mesh Quality Assessment

An overview of the mesh metrics for all the tibia models and the femur model is shown in Table 4.1.

Table 4.1: Mesh Metrics

Part	Number of elements	Element size (mm)
Tibia - 4°	370186	1
Tibia - 5°	367154	1
Tibia - 7°	371108	1
Femur - DO	316226	1

Table 4.2 shows a summary of the shape metrics.

Table 4.2: Shape Metrics

Part	Avg Minimum Angle	Avg Maximum Angle	Aspect Ratio
Tibia - 4°	38.86	87.86	1.63
Tibia - 5°	41.30	85.30	1.52
Tibia - 7°	38.94	87.84	1.61
Femur - DO	38.19	89.01	1.66

As mentioned in Section 3.1.5, the bones were modeled as rigid bodies, a common approach taken in contact analysis of the knee joint. This is done since the material behavior of bones is much stiffer than soft tissues. Hence, the bones were meshed using first-order tetrahedral elements in Hypermesh software. Although the shape metrics of the bones show that the elements are of good quality, the quality of the meshes of bones wasn't of the highest importance for this study since the bones were kept rigid throughout the simulations.

4.2 Effect of Correction Angle on Articular Surface Contact Forces

The contact forces are calculated at the contact surfaces between soft tissues. Table 4.3 shows the values of contact forces at surface pairs (Section 3.3) and Figure 4.2 shows the plots of the contact forces for different correction angles. The distribution of contact forces on the surfaces of the femoral cartilage, medial, and lateral tibial cartilages are shown in Figures 4.3 - 4.5.

Table 4.3: Contact forces between articular surface pairs for different corrections

Surface pairs	Contact forces (N)			
	Uncorrected (0°)	4°	5°	7°
FC-MTC	541.7	528.9	525.5	647.3
FC-LTC	248.6	322.2	339.9	386.9
FC-MM	199.8	122.1	96.4	90.3
FC-LM	5.1	45.3	55.8	84.9

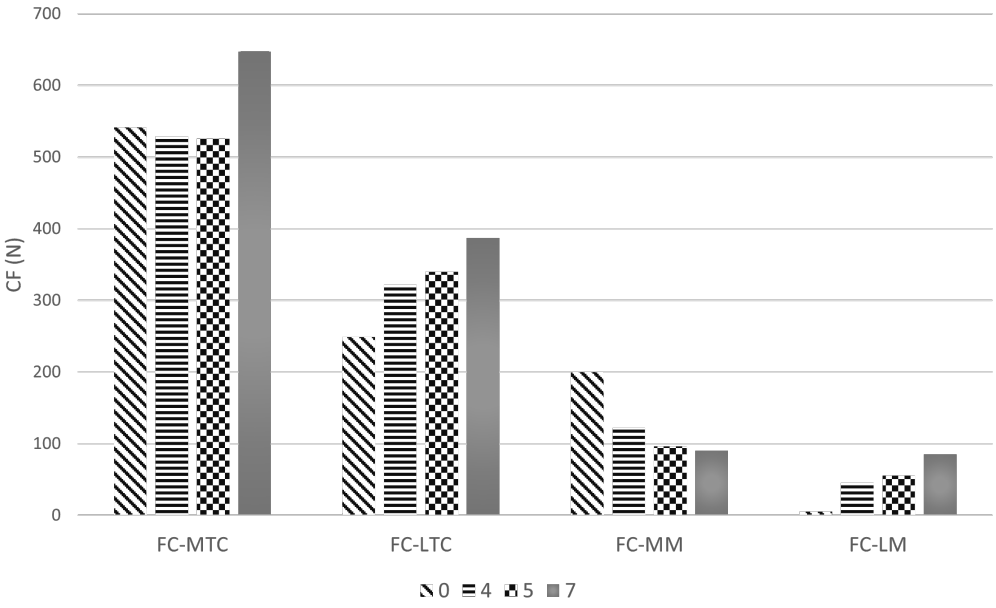


Figure 4.2: Contact forces results at surface pairs for different correction angles



(a) Uncorrected (0°) (b) 4°



(c) 5° (d) 7°

Figure 4.3: Contact force distribution on the femoral cartilage

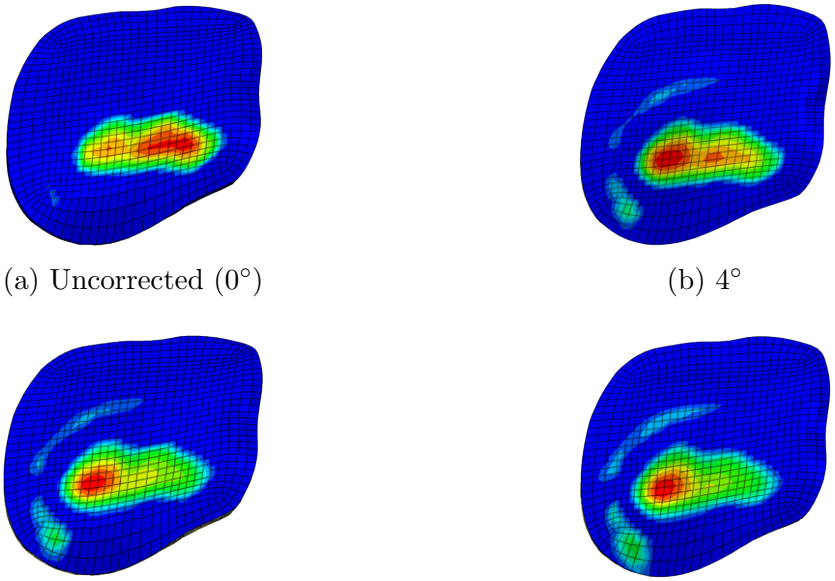


(a) Uncorrected (0°) (b) 4°



(c) 5° (d) 7°

Figure 4.4: Contact force distribution on the proximal surface of medial tibial cartilage



(a) Uncorrected (0°) (b) 4°

(c) 5° (d) 7°

Figure 4.5: Contact force distribution on the proximal surface of lateral tibial cartilage

4.3 Effect of Correction Angle on Articular Surface Peak Contact Pressures

Results of the peak contact pressure outputs on the soft tissues are shown in Table 4.4, and plotted in Figures 4.6 and 4.7. The distribution of contact pressures on the femoral, medial tibial, and lateral tibial cartilages are shown in Figures 4.8 - 4.10.

Table 4.4: Contact pressures on the articular surface for different corrections

Component	Contact pressures (MPa)			
	Uncorrected (0°)	4°	5°	7°
Medial Tibial Cartilage (MTC)	6.383	5.697	5.467	5.430
Lateral Tibial Cartilage (LTC)	3.673	4.489	4.74	5.312
Medial Meniscus (MM)	5.116	4.208	2.867	2.747
Lateral Meniscus (MM)	1.063	2.519	2.825	3.439
Femoral Cartilage (FC) - Medial	6.210	5.657	5.446	5.362
Femoral Cartilage (FC) - Lateral	3.551	4.462	4.602	5.203

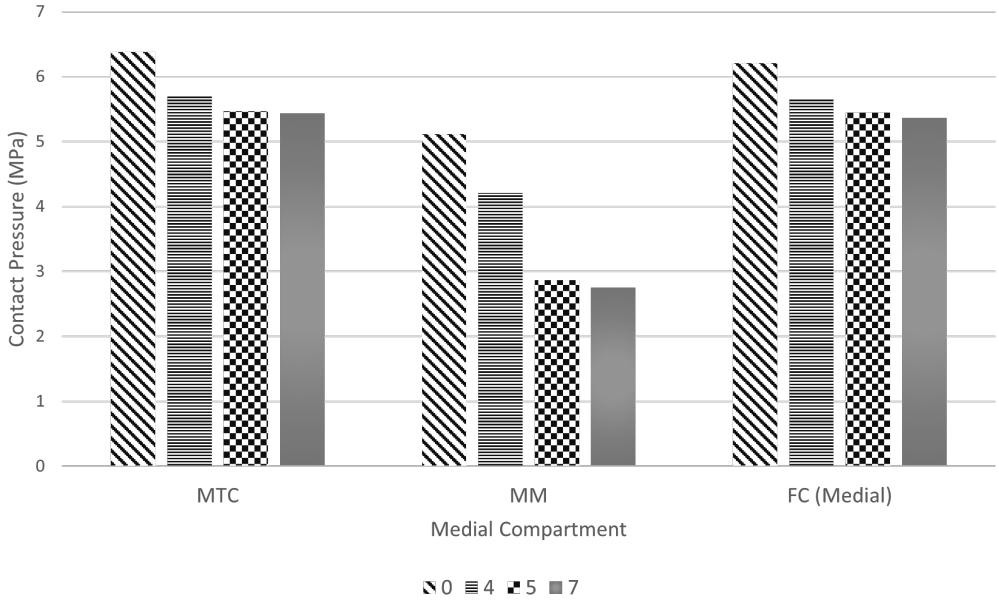


Figure 4.6: Contact Pressures at the medial compartment for different correction angles

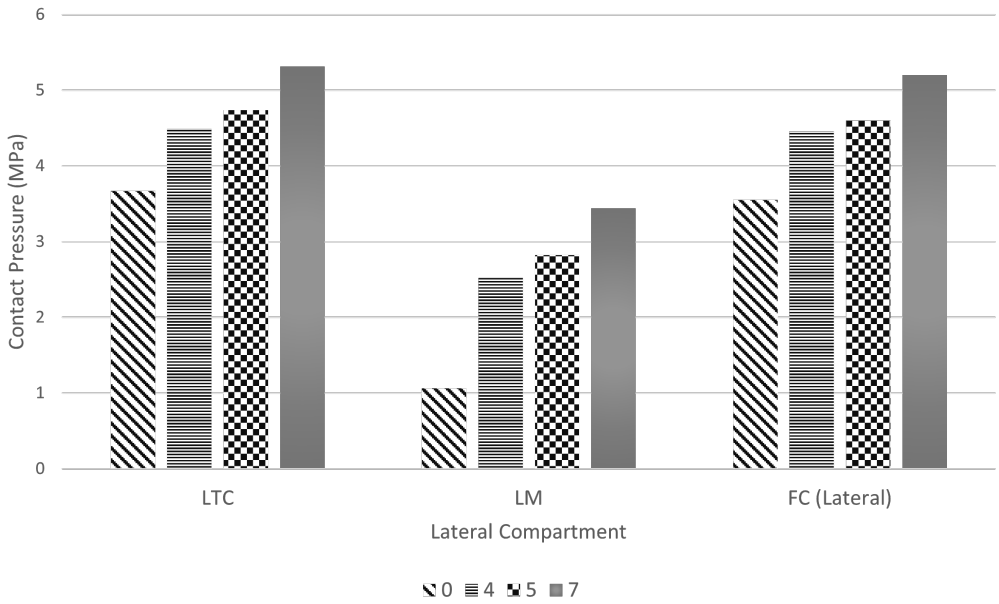
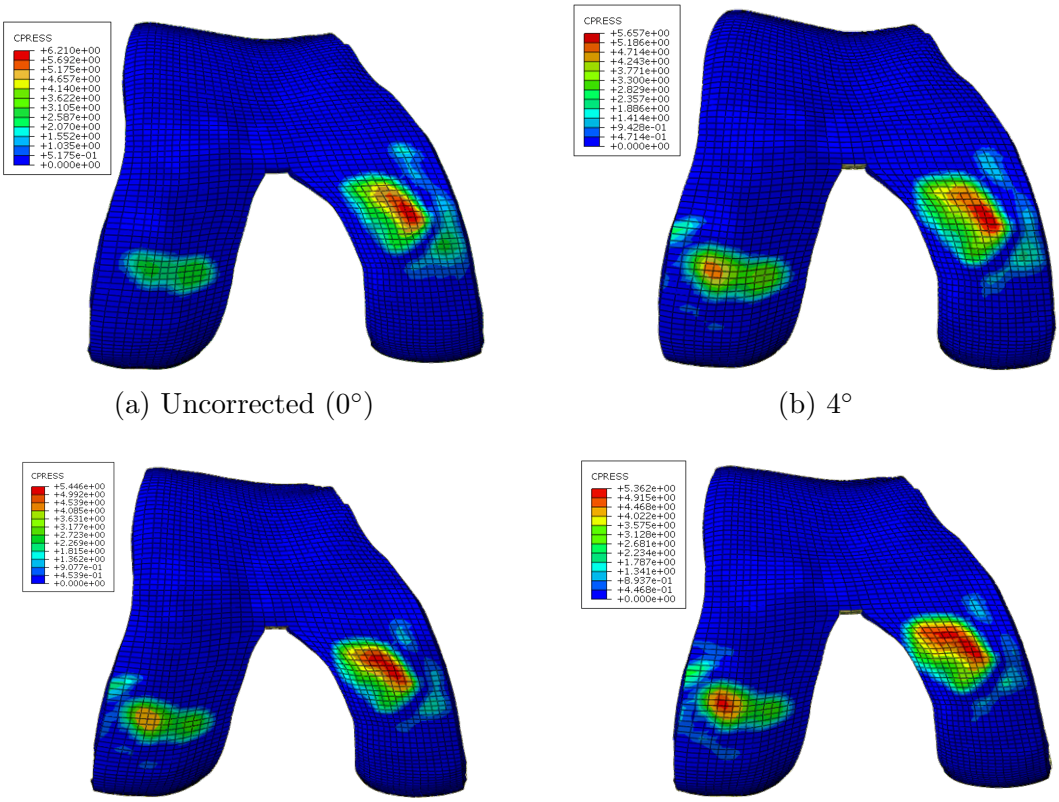


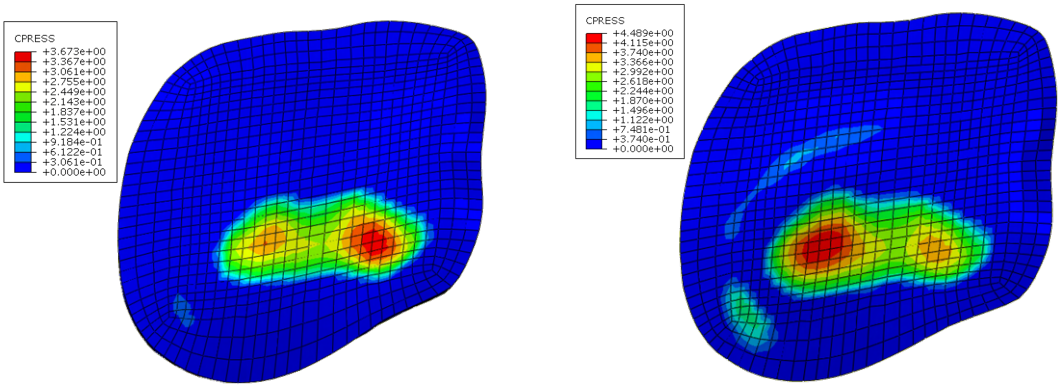
Figure 4.7: Contact Pressures at the lateral compartment for different correction angles



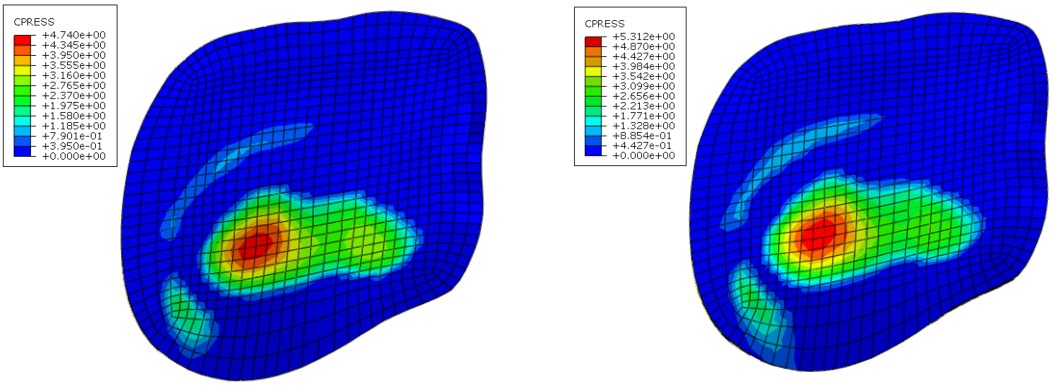
(a) Uncorrected (0°) (b) 4°

(c) 5° (d) 7°

Figure 4.8: Contact Pressure distribution on the femoral cartilage

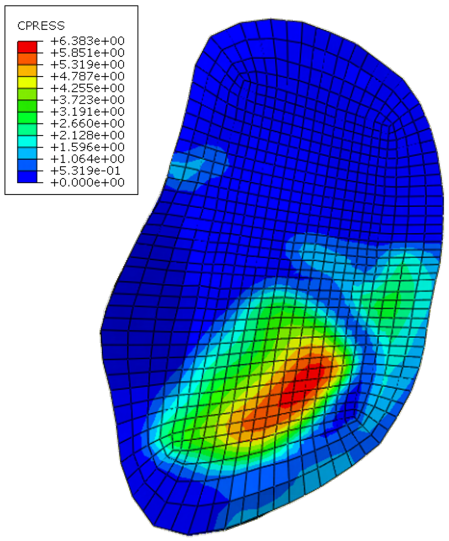


(a) Uncorrected (0°) (b) 4°

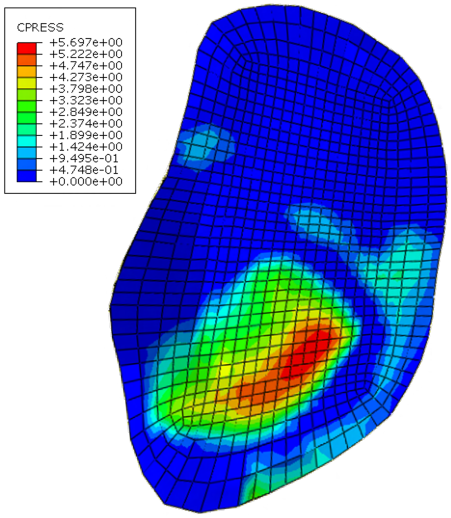


(c) 5° (d) 7°

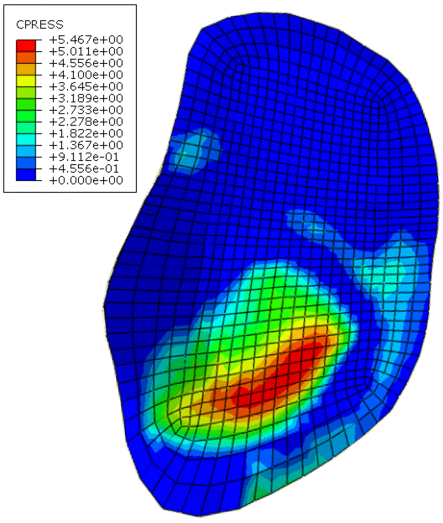
Figure 4.9: Contact Pressure distribution on the proximal surface of lateral tibial cartilage



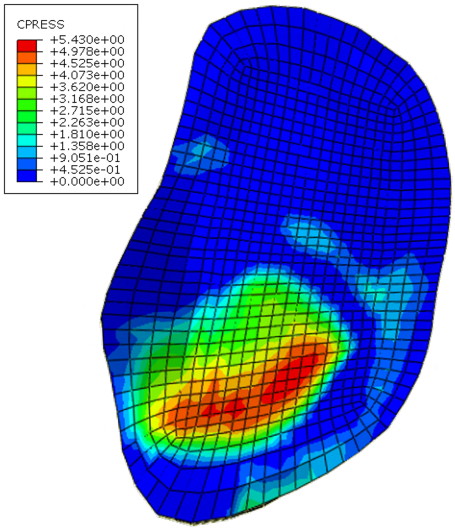
(a) Uncorrected (0°)



(b) 4°



(c) 5°



(d) 7°

Figure 4.10: Contact Pressure distribution on the proximal surface of medial tibial cartilage

4.4 Effect of Correction Angle on the stress distribution across the articular surface

The Von Mises equivalent stresses were obtained to observe the stress distribution across the articular surface The results are shown in Table 4.5, and plotted in Figures 4.11 and 4.12. The distribution of stress on the femoral, medial tibial, and lateral tibial cartilages are shown in Figures 4.13 - 4.15.

Table 4.5: Stress distribution across the articular surface for different corrections

Component	Von Mises Stresses (MPa)			
	Uncorrected (0°)	4°	5°	7°
Medial Tibial Cartilage (MTC)	2.976	2.632	2.571	2.479
Lateral Tibial Cartilage (LTC)	1.986	2.321	2.427	2.694
Medial Meniscus (MM)	3.410	3.034	2.782	2.308
Lateral Meniscus (MM)	0.876	1.960	2.155	2.884
Femoral Cartilage (FC) - Medial	2.979	2.608	2.568	2.455
Femoral Cartilage (FC) - Lateral	1.723	1.967	2.030	2.233

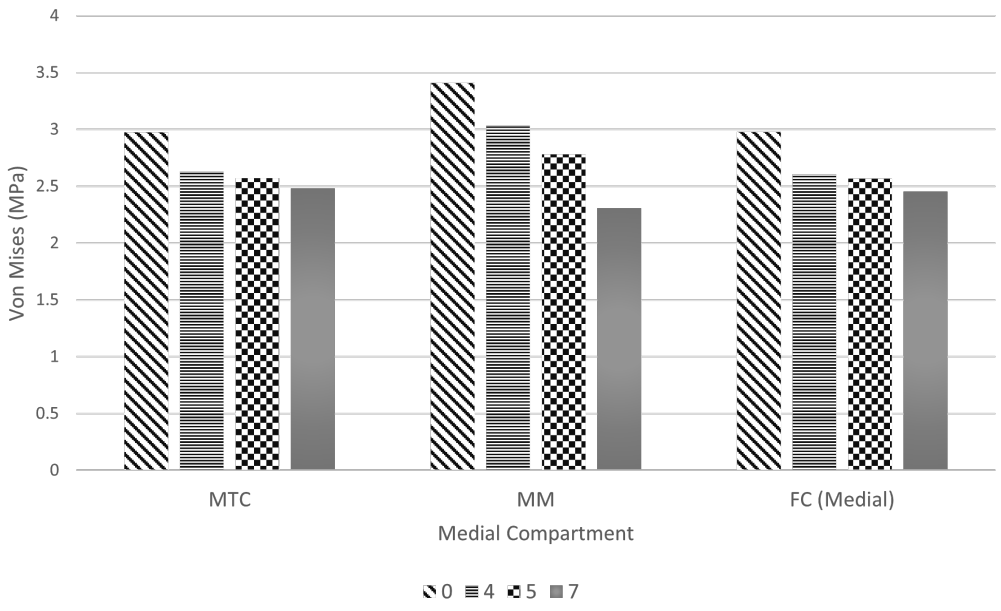


Figure 4.11: Von Mises stresses at the medial compartment for different correction angles

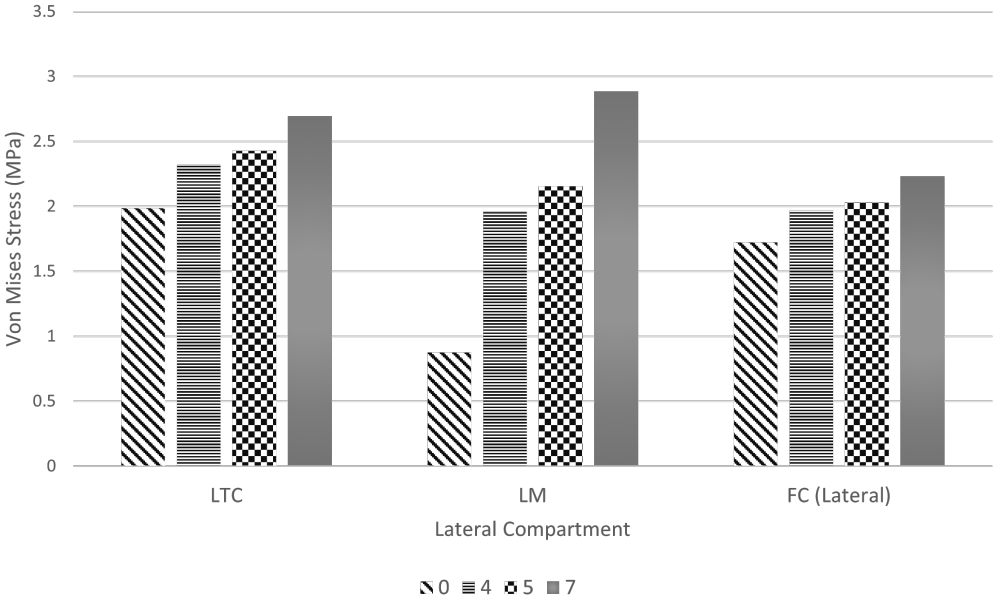
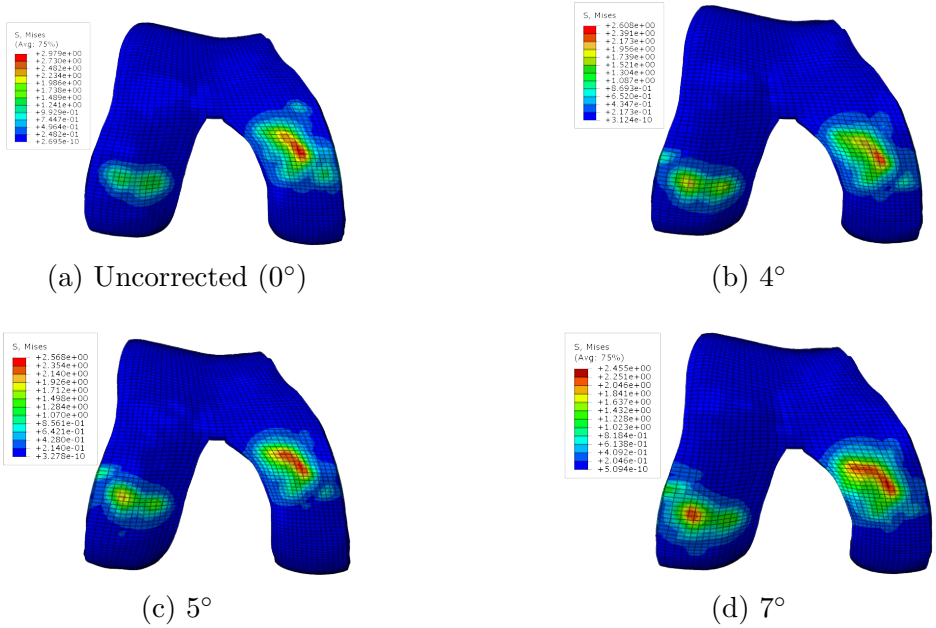


Figure 4.12: Von Mises stresses at the lateral compartment for different correction angles



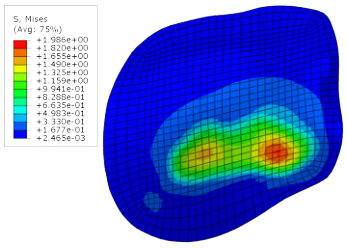
(a) Uncorrected (0°)

(b) 4°

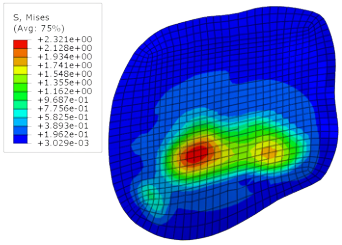
(c) 5°

(d) 7°

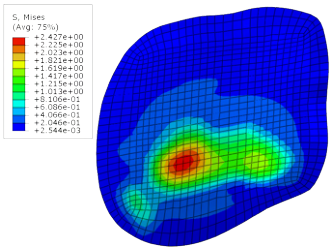
Figure 4.13: Von Mises stress distribution on the femoral cartilage



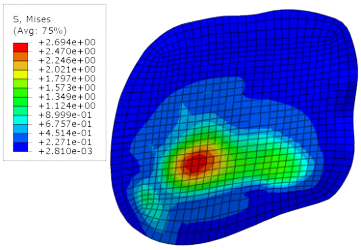
(a) Uncorrected (0°)



(b) 4°

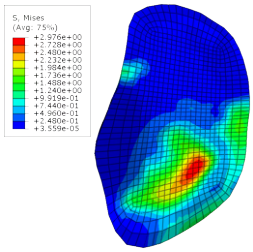


(c) 5°

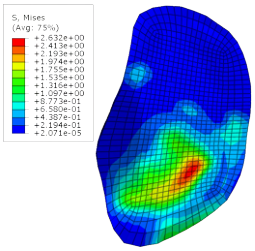


(d) 7°

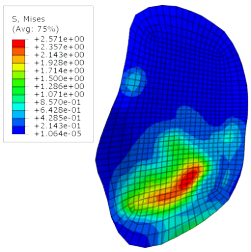
Figure 4.14: Von Mises stress distribution on the proximal surface of lateral tibial cartilage



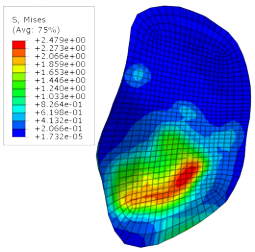
(a) Uncorrected (0°)



(b) 4°



(c) 5°



(d) 7°

Figure 4.15: Von Mises stress distribution on the proximal surface of medial tibial cartilage

4.5 Effect of Correction Angle on MCL Strain

The impact of varying the correction angle on the strain experienced by the MCL is analyzed and documented. The strain in the MCL is represented by the force exerted on the spring elements. 4.16 illustrates the strain distribution across each MCL element as well as the overall force exerted. This detailed representation allows for a comprehensive understanding of how different correction angles affect the mechanical response of the MCL, providing insights into the optimal correction strategies for minimizing strain and enhancing joint stability.

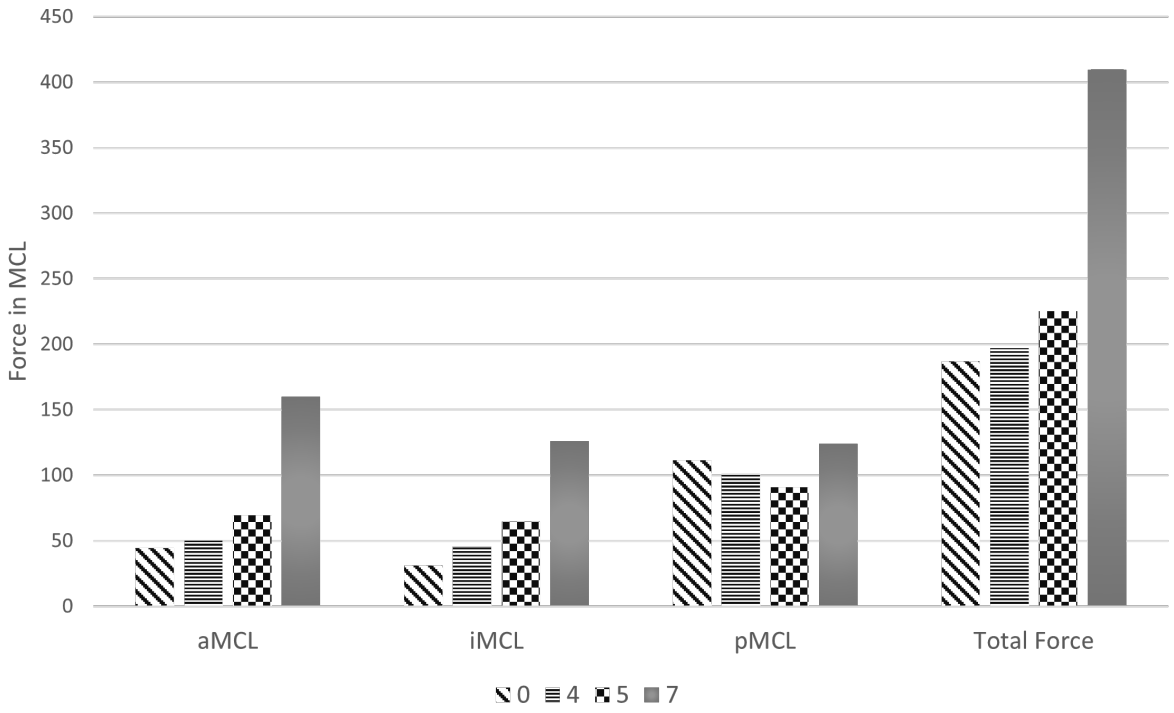


Figure 4.16: Effect of Correction Angle on Force in MCL

4.6 Effect of Release of the Superficial MCL on the Articular Surface Contact Force, and Pressure distributions

In this study, partial and total releases of the superficial MCL were performed on a 5° correction model to evaluate its viability as a surgical technique for reducing medial contact pressures. The release sequence began with first deleting the spring element of the intermediate MCL, followed by the anterior and posterior MCLs. The results are summarized in Tables 4.6 and 4.7. Corresponding plots are presented in Figures 4.17 - Figures 4.19.

Table 4.6: Contact forces between articular surface pairs due to partial and total MCL release. The numbers represent contact forces in Newtons (N).

Surface pairs	MCL Intact	Partial release		Total release
		iMCL	iMCL+aMCL	iMCL+aMCL+pMCL
FC-MTC	525.5	455.7	385.3	290.6
FC-LTC	339.9	357.8	374.5	408.4
FC-MM	96.4	81.1	68.7	48.8
FC-LM	55.8	60.9	63.6	71.7

Table 4.7: Contact pressures on the articular surface as a result of partial and total MCL release

Component	Contact pressures (MPa)			
	MCL Intact	iMCL	iMCL+aMCL	Total release
Medial Tibial Cartilage (MTC)	5.467	5.031	4.660	4.165
Lateral Tibial Cartilage (LTC)	4.740	4.929	5.062	5.364
Medial Meniscus (MM)	2.867	2.366	1.981	1.603
Lateral Meniscus (MM)	2.825	2.875	2.897	3.131
Femoral Cartilage (FC) - Medial	5.446	4.992	4.531	3.955
Femoral Cartilage (FC) - Lateral	4.602	4.778	4.908	5.204

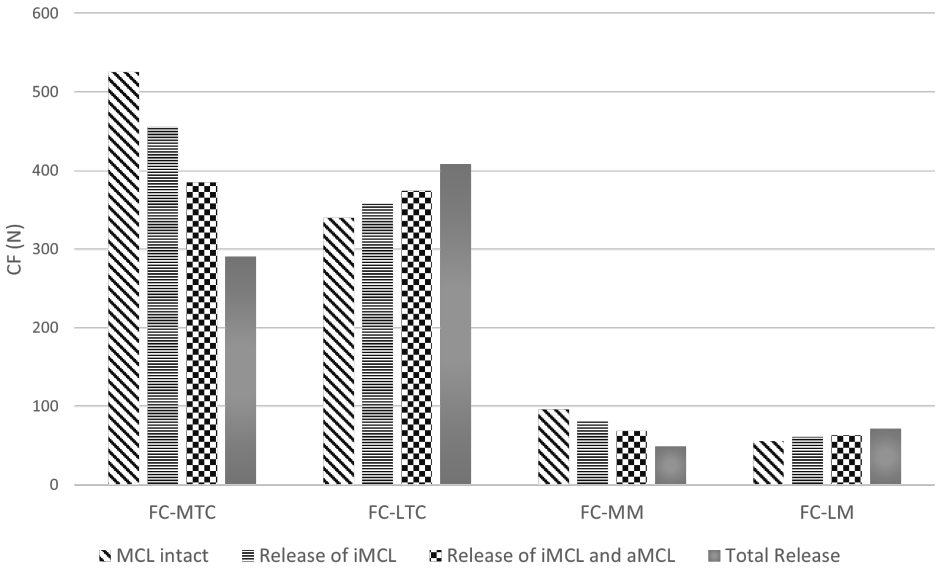


Figure 4.17: Effect of MCL release on Contact Force between surface pairs

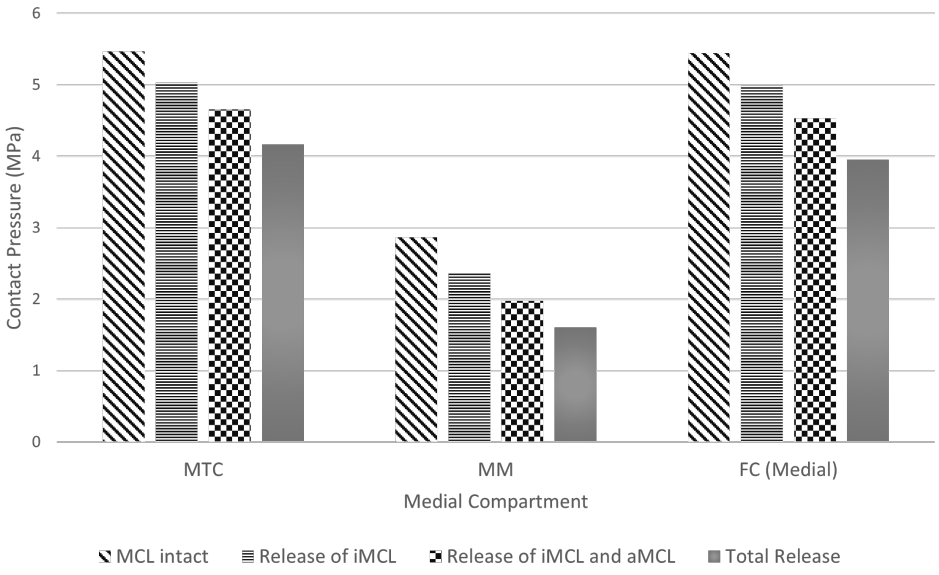


Figure 4.18: Effect of MCL release on Contact Pressure distribution across the medial compartment for 5° correction

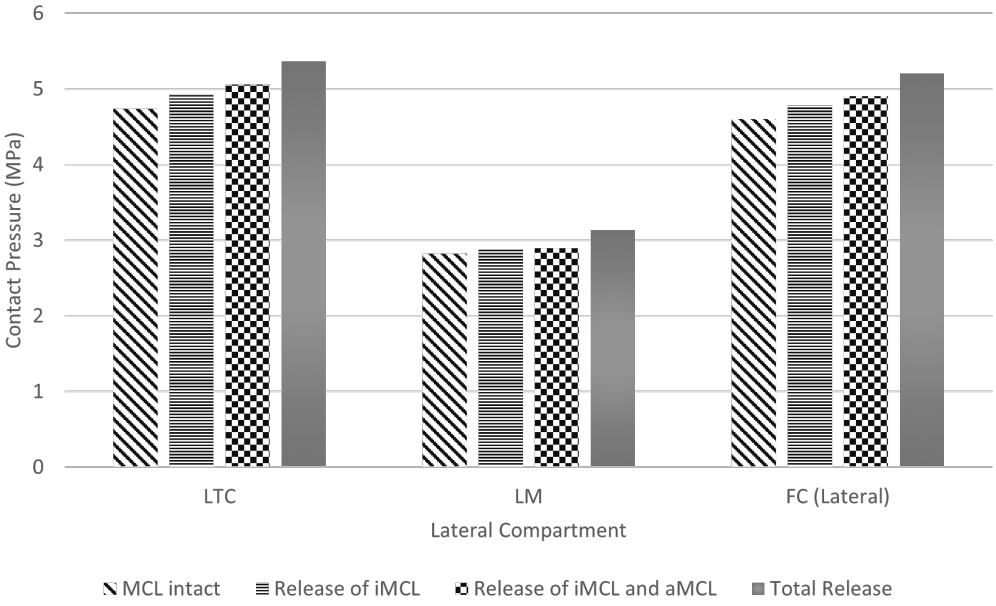


Figure 4.19: Effect of MCL release on Contact Pressure distribution across the lateral compartment for 5° correction

4.7 Results of Double Osteotomy

FE analysis for a double osteotomy procedure was carried out for 7° overall correction to determine articular surface contact and stress parameters. The model development process included a combination of lateral closing wedge osteotomy at the femur and an opening wedge high tibial osteotomy. The results were compared with the HTO model with 7° correction. The results obtained are shown in Tables 4.8 - 4.10. The plots for the same are shown in Figures 4.20 - 4.24.

Table 4.8: Contact Force comparison between HTO at 7° correction and Double Osteotomy

Surface Pairs	Contact Force (N)	
	HTO at 7°	Double Osteotomy
FC-MTC	647.3	270.7
FC-LTC	386.9	405.1
FC-MM	90.3	41.5
FC-LM	84.9	80.6

Table 4.9: Contact Pressure comparison between HTO at 7° correction and Double Osteotomy

Component	Contact Pressure (MPa)	
	HTO at 7°	Double Osteotomy
Medial Tibial Cartilage (MTC)	5.43	2.82
Lateral Tibial Cartilage (LTC)	5.312	5.249
Medial Meniscus	2.747	1.385
Lateral Meniscus	3.439	3.523
Femoral Cartilage (FC) - Medial	5.362	2.741
Femoral Cartilage (FC) - Lateral	5.203	5.115

Table 4.10: Von Mises Stress comparison between HTO at 7° correction and Double Osteotomy

Component	Von Mises Stress (MPa)	
	HTO at 7°	Double Osteotomy
Medial Tibial Cartilage (MTC)	2.479	1.360
Lateral Tibial Cartilage (LTC)	2.694	2.667
Medial Meniscus	2.308	1.019
Lateral Meniscus	2.884	2.936
Femoral Cartilage (FC) - Medial	2.455	1.251
Femoral Cartilage (FC) - Lateral	2.233	2.215

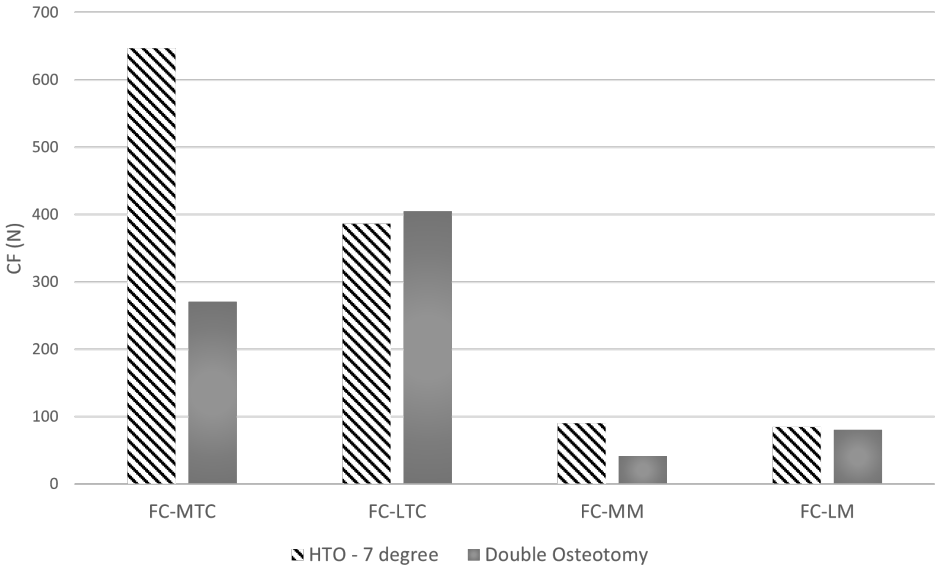


Figure 4.20: Contact Force comparison between HTO at 7° correction and Double Osteotomy

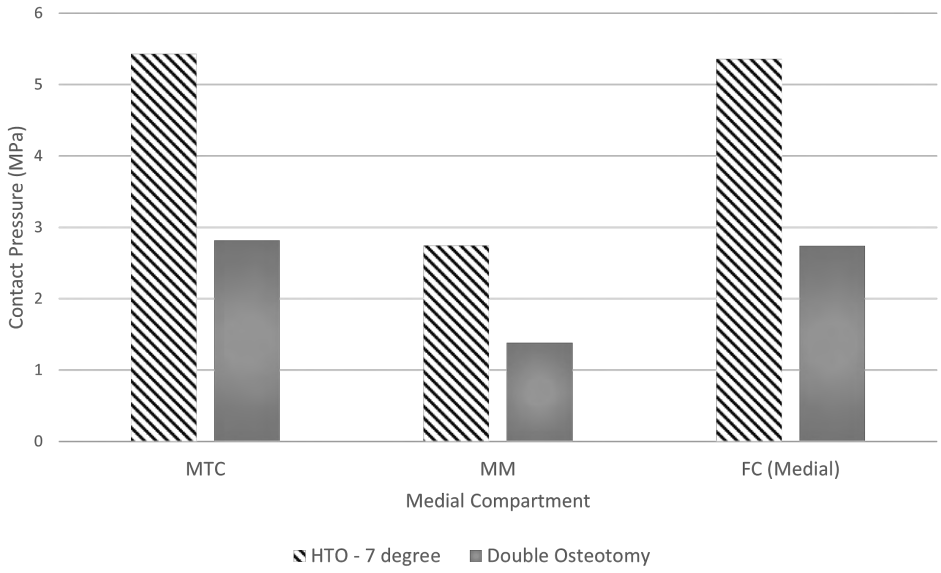


Figure 4.21: Contact Pressure comparison between HTO at 7° correction and Double Osteotomy on the medial compartment

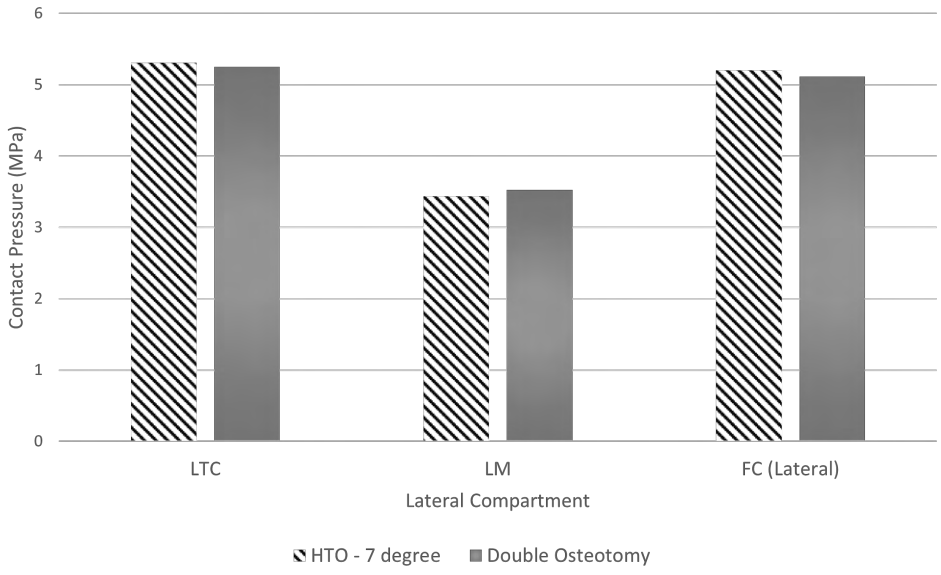


Figure 4.22: Contact Pressure comparison between HTO at 7° correction and Double Osteotomy on the lateral compartment

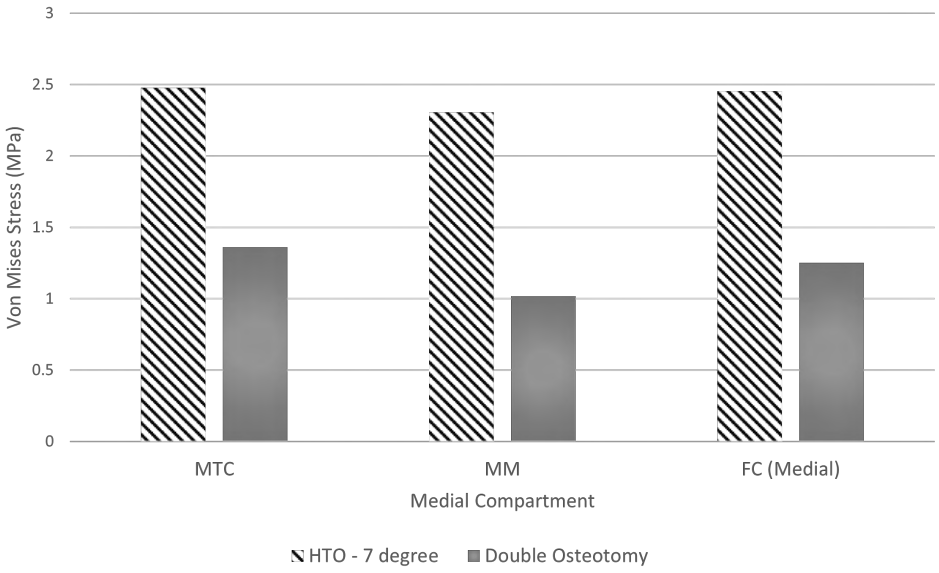


Figure 4.23: Von Mises Stress comparison between HTO at 7° correction and Double Osteotomy on the medial compartment

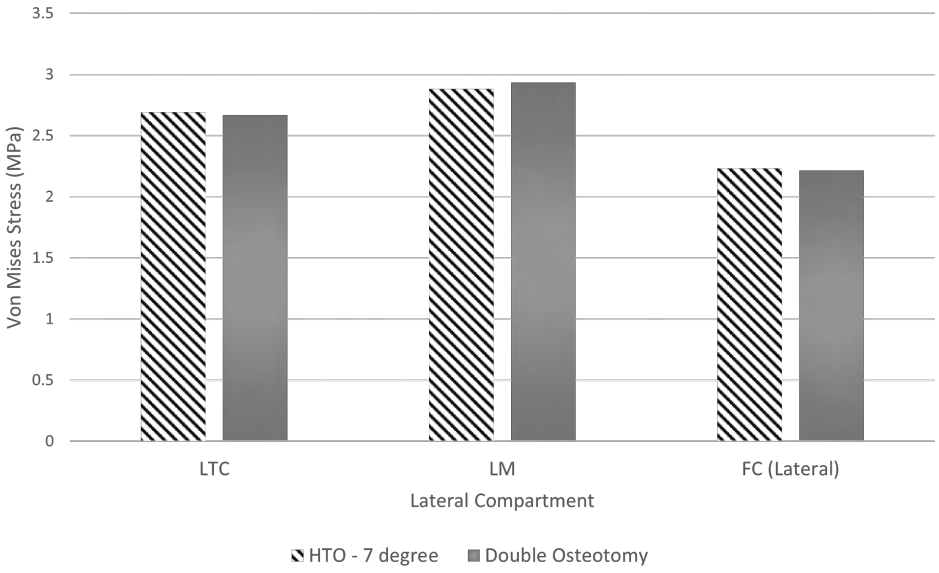


Figure 4.24: Von Mises Stress comparison between HTO at 7° correction and Double Osteotomy on the lateral compartment

Chapter 5

Discussion

The study aimed to develop finite element models of the knee joint to simulate the HTO surgical procedure. The primary objective of this study was to investigate how the change in knee alignment affects the contact forces and pressures on the articular surface of the knee joint, for under-correction, optimal correction, and overcorrection. In addition, the study aimed to quantify the MCL strain at different osteotomy corrections and the implications of MCL release on the articular surface of the knee joint. A double osteotomy procedure was also simulated to analyze its efficacy against a single osteotomy procedure. The chapter aims to comprehensively analyze all the results generated by comparing and validating with existing literature.

5.1 Development of FE Model

Surgical Simulation of HTO

The models for tibia generated for HTO are based on a completely novel procedure that takes into account key aspects of lower limb mechanics. As mentioned in Section 3.1.3, the corrections at the tibia were made by splitting the tibia about a cutting axis, removing a small wedge at the lateral side, and subsequently rotating the distal end of the tibia to achieve the desired correction. Although this procedure is typically not how the surgery is performed in a clinical scenario, it allows for the shift in the mechanical axis of the lower limb, which is an integral part of unloading the knee joint during an osteotomy procedure. Moreover, the procedure adopted emulates a healed HTO, which is crucial for the analysis of post-operative conditions. A long-standing anteroposterior radiograph was utilized in

combination with the model developed by Rao [72] to determine the desired correction of 5°, based on a pre-planning procedure by Miniaci et al [55]. This method was adopted due to the unavailability of the MRI of the entire length of the lower limb. With the optimal correction angle determined, the remaining models were developed based on the same procedure and were termed as under correction and overcorrection.

A common approach adopted by researchers [16, 32, 40, 51] to model the tibia for HTO is by removal of a wedge on the medial side of the tibia without performing the opening of the osteotomy. An approach like this, although could save computational time and could be used for analysis targeting aspects like hinge stress and fractures, and fixation plate stresses, is not a feasible approach for articular surface contact analysis. This is because this procedure does not emulate the clinical scenario of HTO since it does not shift the mechanical axis of the tibia, which is crucial for investigating contact and loading parameters.

5.2 Finite Element Analysis

5.2.1 Validation of FE model

The FE knee model was validated by comparing the tibiofemoral contact pressure results for the uncorrected model with existing literature on contact forces and pressures. The validation process involved using two different material properties for the cartilage: one with a modulus of 20 MPa [3], and the other with a modulus of 5 MPa [68]. Both models were subjected to a load of 800N as described in Section 3.2.1 and the same boundary conditions were maintained.

The maximum contact pressure results for the model with higher cartilage modulus of elasticity was found to be 6.383 MPa. The results for the first model lie within the range reported by Huang et al [37], where the peak contact pressure on the knee joint was reported to be 7.31 ± 2.41MPa. The peak contact pressures generated for the model with the lesser modulus of elasticity for cartilage were found to be 2.325MPa on the medial compartment and the peak lateral compartment contact pressure was 2.581MPa. The results are within the range of results generated by Donahue et al [25], where the maximum pressure on the medial compartment was 2.55MPa and 2.26 MPa on the lateral compartment. The difference in the results between the first model and Danoahue et al could be due to a difference in cartilage thickness, or a difference in the material property used. A study by Li et al [46] shows that a 10% alteration in the cartilage layer thickness led to a corresponding

10% variation in surface pressure within a tibiofemoral joint model. It was also stated that the variation in material properties significantly affects the stress distribution across the tibial plateau. However, the consistency between the contact pressure results in this study and the literature data indicates that the FE model can produce reasonable results.

5.2.2 Effect of varying correction angle on the articular surface and MCL strain

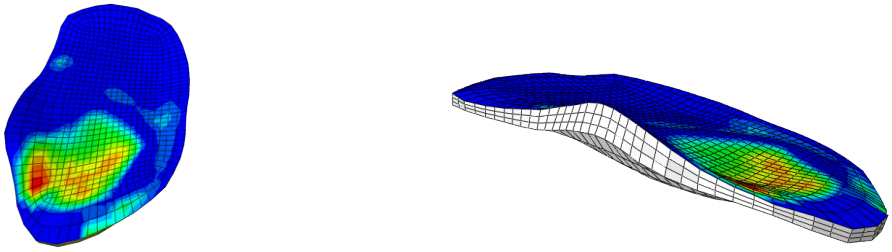
Contact forces

Determining contact forces on the articular surface provides crucial information on how the joint loading is affected as the load-bearing axis is shifted. The primary purpose of an open wedge HTO surgery is to effectively unload the affected compartment, typically the medial compartment in cases of medial knee OA, and to shift the loading laterally. Optimal corrections could create a more balanced distribution of load across the knee joint, alleviating symptoms and potentially slowing the progression of OA. The findings of this study reported in Section 4.2 provided crucial information on how the joint is unloaded as the load-bearing axis is shifted laterally. Specifically, the redistribution of forces helps in understanding how the altered alignment influences the load distribution on the cartilage.

The contact force on the medial compartment decreased by 2% for a 4-degree correction and 3% for a 5-degree correction. On the contrary, the contact force on the lateral compartment increased by 29%, 37%, and 55% for 4, 5, and 7 degrees of correction, respectively. It was hypothesized that increasing the correction angle would lead to a decrease in medial compartment forces and a corresponding increase in the load distribution across the lateral compartment. Figures 4.3, 4.4, and 4.5 illustrate contour plots of the load distribution across the femoral cartilage, medial tibial cartilage, and lateral tibial cartilage. The red areas in these figures represent regions of high load intensity.

What is evident from these images is that the areas with higher intensity on the medial side of the femoral cartilage and the medial tibial cartilage gradually decrease and shift laterally with increasing correction angles. In contrast, the load distribution on the lateral side of the femoral cartilage and the lateral tibial cartilage intensifies and also shifts laterally as the correction angle increases. This distribution pattern supports the initial hypothesis that the intensity of loading would decrease on the medial side and increase on the lateral side. Therefore, the results effectively demonstrate the efficacy of HTO surgery in unloading the medial compartment.

However, a 20% rise in the contact force was observed on the medial tibial cartilage in the 7° correction model. One explanation is possible due to the geometry of the cartilage itself. As shown in Figure 5.1b, the lateral aspect of the medial tibial cartilage has an elevated surface, creating a ridge where the load intensity is higher. The increase in contact force on the medial tibial cartilage for the 7° correction could be due to the increase in contact area between the femoral cartilage and the medial tibial cartilage. This change in the contact area is not as evident in the 5° model but spikes in the 7°, as plotted in Figure 5.2, potentially explaining the increased contact loading.



(a) Load distribution on MCL for 7° correction

(b) Elevated surface creating a ridge on the MTC where loading is higher

Figure 5.1: Geometry of medial tibial cartilage and load distribution on 7° correction

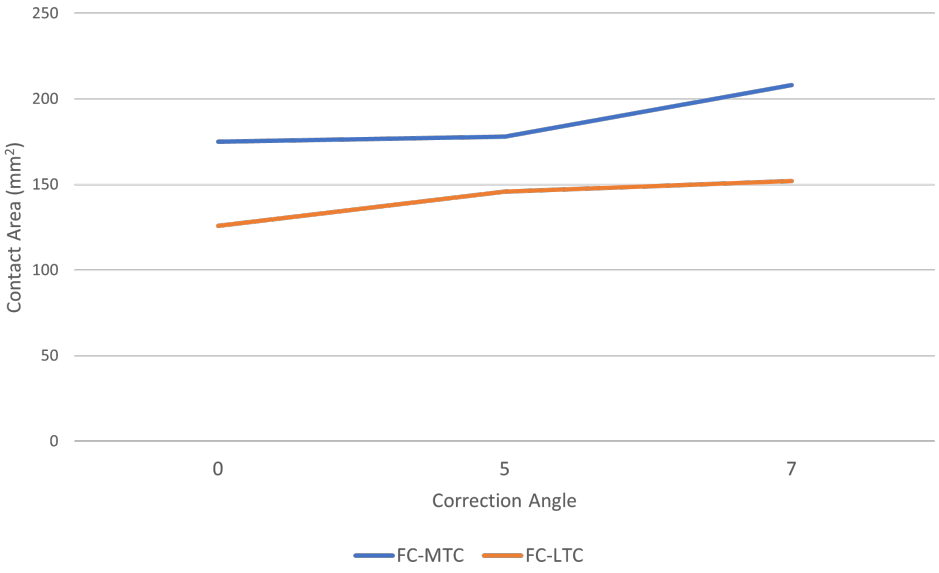


Figure 5.2: Change in contact area in medial and lateral compartments

However, this abnormal force distribution may indicate the implications of overcorrection. As shown in Figure 4.16, the total force in the MCL spikes in the overcorrected model. This increase in MCL strain creates a region of abnormal force distribution on the medial compartment, suggesting that overcorrection leads to uneven pressure distributions across the tibial plateau. Therefore, it is critical to maintain the correction angle within an optimal range to achieve the best clinical outcomes and avoid potential complications associated with overcorrection.

Contact pressures and stress distributions

It was hypothesized that the peak contact pressure would decrease medially and increase laterally in the knee joint by shifting the load-bearing axis. Section 4.3 reported the peak contact pressures in the knee joint, and the findings of this study supported the hypothesis. The peak contact pressure in the medial tibial cartilage decreased from 6.383 MPa in the uncorrected tibia to 5.43 MPa in the overcorrected (7°) model, representing a 15% reduction. The optimal correction angle of 5° resulted in a peak contact pressure of 5.467 MPa in the medial tibial cartilage, a 14% reduction. Conversely, the peak contact pressure in the lateral tibial cartilage increased from 3.673 MPa to 5.312 MPa in the overcorrected (7°) model, a 45% increase, and 4.74 MPa in the optimal correction model (29% increase). On the medial side of the femoral cartilage, there was a decrease from 6.21 MPa to 5.446 MPa for optimal correction (12% decrease), and for the overcorrection, a 14% decrease was observed. The lateral side of the femoral cartilage saw a decrease The model with under-correction (4°) showed an 11% decrease in medial tibial cartilage pressure and a 9% decrease in medial femoral cartilage pressure. The pressure distributions across the articular surface are shown in Figures 4.8, 4.9, and 4.10. The distribution indicates a lateral shift in the high-pressure regions as the corrections increase.

The Von Mises stress variations across the articular surface showed a similar trend in distribution across the articular as the correction angle increased. The stress reduction across the medial tibial cartilage were 11%, 13%, and 17% for 4°, 5°, and 7° corrections, respectively. The reductions across the medial side of the femoral cartilage were 12%, 14%, and 17.50%. On the lateral compartment, the stress on the lateral cartilage increased by 17% for 4°, 22% for 5°, and 35% for 7°, and 14%, 18%, and 30% on the lateral side of the femoral cartilage.

These results suggest that varying degrees of correction angles can significantly impact the distribution of contact pressures within the knee joint, thereby affecting the mechanical environment of the knee joint post-surgery. The correction angle of 5° emerged as the balanced optimal correction, offering a substantial reduction in medial pressure while

avoiding excessive increases in lateral pressure. This balance is crucial for maintaining joint homeostasis and preventing new areas of degeneration. The decrease in femoral cartilage pressure across different correction models further supports the notion that HTO can beneficially alter joint mechanics.

The findings of this study are in line with the reported literature targeting contact pressures and stresses on the articular surface as a result of shifting the load-bearing axis. The results obtained for contact pressures are very comparable to the study by Mina et al [54], who also reported that as the correction angle increases, the contact pressures decrease on the medial compartment and shift laterally. The study suggested that a correction of 4° was recommended for optimal pressure distribution across the medial and lateral compartments. The stress distribution reported in this study correlates with Trad et al [84]. Although their study performed a lateral closed wedge osteotomy on the tibia, the objective was similar: shift the load-bearing axis laterally. The study reported a shift in Von Mises stress distribution towards the lateral compartment, and suggested that at a correction of 4.5°, a balanced distribution of stresses between the two compartments was noticed. Zhang et al [89] reported similar trends in the variation of stresses across the articular surface. The optimal results for their model were seen at 7.5°, with stresses most uniformly distributed between these two compartments at this correction. The choice of optimal correction, although different than the ones reported, lies well within the range reported in the literature.

MCL Strain

While the contact force and pressure distributions across the medial compartment decrease after osteotomy, the strain in MCL increases. Clinically, this occurs because the superficial MCL, which overlies the osteotomy site, gets stretched during the opening of the osteotomy. This stretching happens as the bone cut during the procedure creates a gap, leading to an elongation of the MCL, thus increasing its strain.

In the study, the strain in the MCL was quantified as a function of the force in ligament spring elements. Specifically, three spring elements were modeled to represent the superficial MCL: the anterior (aMCL), intermediate (iMCL), and posterior (pMCL) portions.

The primary objective was to measure the force in the MCL, and the results are depicted in Figure 4.16. The findings indicate that with increased correction achieved through osteotomy, the force, and consequently the strain, in the superficial MCL significantly rises. Specifically, the total MCL force escalates from 187N in an uncorrected tibia to 410N in an overcorrected model, marking a 120% increase. For an optimally corrected

tibial model, the total force increases to 225N, still reflecting a notable rise in MCL strain. Egmond et al [86] reported in their cadaveric study that the MCL tension increases by an average of 203N after osteotomy, and relaxes over time but remains in a constant state of stress which ultimately leads to increased contact pressures. The results from this study align with these findings, showing similar trends in MCL force. The tensile strength of the MCL is reported to be 534N approximately [73], so an increase of this magnitude in the MCL after correction is substantial and could lead to potential complications.

The increase in MCL force and strain can be attributed to the biomechanical changes introduced by the osteotomy opening. As the alignment of the tibia is achieved, the medial compartment, which previously absorbed a greater portion of the load, experiences a reduction in contact force and pressure. However, this load reduction in the medial compartment shifts the strain to the MCL, causing it to bear more force. Although the medial tibial cartilage experiences reduced contact force and stress, this reduction is insufficient to offset the abnormal loading of the MCL. A more significant reduction in contact force and pressure in the medial compartment could be achieved by partially or fully releasing the MCL. This release could help distribute the load more evenly across the joint and reduce the strain on the MCL.

5.2.3 Effect of MCL Release on articular surface force and pressure distributions

There is an ongoing debate among researchers and clinicians regarding the efficacy of releasing the MCL after osteotomy to reduce joint loading in the medial compartment. This debate focuses on whether releasing the MCL is a viable option to reduce medial compartment contact forces and pressures and, if so, whether a partial release is sufficient or if a complete release is necessary. The study aimed to quantify the effects of both partial and total release of the superficial MCL on the articular surface contact force and pressures for a 5° correction. These findings are detailed in Section 4.6. For the sake of discussion, the release of only the iMCL will be termed as condition 1, the release of iMCL and aMCL will be termed as condition 2, and total release as condition 3.

The results indicate that the contact force on the medial tibial cartilage was reduced by 13% for condition 1, 27% for condition 2, and 48% for condition. Similarly, the contact pressures on the medial tibial cartilage showed reductions of 8%, 15%, and 24% for conditions 1, 2, and 3 respectively. On the lateral tibial cartilage, the contact forces increased by 5%, 10%, and 20% for the release conditions when compared with results with intact MCL. The contact pressures on the lateral tibial cartilage increased by 4%, 7%, and 13%.

On the femoral cartilage, the medial side saw a decrease of 8%, 17%, and 27% in the contact pressures, and on the lateral side, the pressures increased by 4%, 7%, and 13%. The comparison between the medial and lateral side contact pressures is shown in Figure 5.2.

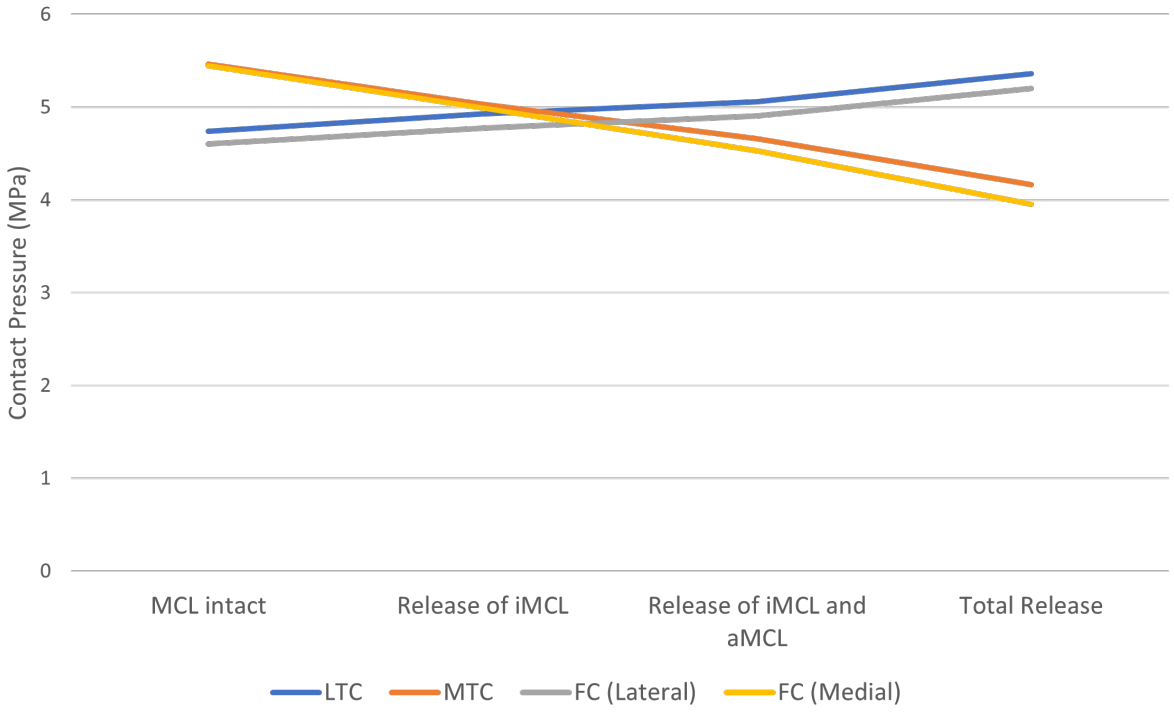


Figure 5.3: Comparison between contact pressure on the medial and lateral compartments for MCL release conditions

The results indicate that the force and pressure distributions across the medial compartment substantially decrease with the total release of the MCL. The effect of the MCL release on the medial side is much greater than on the lateral side. These findings suggest that the release of the MCL can be an effective surgical intervention to further reduce pressures on the medial compartment, potentially improving patient outcomes by slowing the progression of medial compartment OA. The choice of whether to release the MCL partially or completely could be made through appropriate patient selection and degree of deformity. In Figure 5.2, the balance of load between the medial and lateral compartments is noticed after releasing the intermediate MCL, and the gap between the pressure increases with subsequent release conditions. In situations like this, the increase in force and pres-

sure on the lateral side must be taken into account, as they could lead to complications such as valgus laxity in the lateral compartment over time.

The results obtained are comparable with Agneskirchner et al [2] and Egmond et al [86]. Both works of literature reported a decrease in the mean contact pressure and peak contact pressures in the medial compartment and a significant increase in the mean and peak contact pressures in the lateral compartment with the release of MCL. Agneskirchner et al's [2] findings reported a 27% decrease in the peak contact pressures in the medial compartment for 50% release of MCL and a 62% decrease in the peak contact pressures for 100% release of the MCL. Egmond et al [86] reported that a complete release of the superficial MCL results in a significant decrease of the mean contact pressures, and peak contact pressures in the medial compartment, and a significant increase in the lateral compartment. They also reported that a complete release of the superficial MCL results in valgus laxity. Pape et al [65] reported that the release of superficial MCL should be kept to a minimum to decrease the potential of valgus laxity.

5.2.4 Double Osteotomy

Nakayama et al [60] suggested that for large corrections, it is viable to consider a double-level osteotomy to avoid detrimental stresses. The double osteotomy procedure was performed for a 7° correction, and results were compared with a single-level osteotomy. From the results, it is evident that the double osteotomy procedure significantly reduces the forces and pressures across the medial compartment when compared with the results of a single osteotomy. Contact pressures in the medial side of femoral cartilage decreased by 48%, 49% in the medial meniscus, and 48% in the medial tibial cartilage. The contact force on the medial compartment was reduced by 58% at the contact between the femoral cartilage and the medial tibial cartilage. The stress distribution saw a decrease of 49% in the medial side of femoral cartilage, 56% in the medial meniscus, and 45% in the medial tibial cartilage.

Interestingly, the study found that the changes in the lateral compartment were not as profound. This suggests that the double osteotomy does not significantly affect the lateral side of the knee, which typically remains the unaffected compartment in most osteotomy procedures. The stability and function of the lateral compartment are maintained, which is important for overall knee joint function and patient mobility.

These findings highlight the potential benefits of a double osteotomy procedure in reducing the pressures on the knee joint, thereby promoting better clinical outcomes for patients undergoing high tibial osteotomy for larger corrections. Nakayama et al's findings

support the use of double-level osteotomy for large corrections, as it offers a method to achieve the necessary angular correction while mitigating the risk of excessive stress on the medial compartment. This makes it a potentially viable option for patients requiring significant correction without compromising the integrity of the lateral compartment and to prevent complications such as joint line obliquity [7].

5.3 Significance of current study

The study has a multifaceted significance, which includes biomechanical insights, and clinical implications. The FE models developed for this study address key aspects of the biomechanical effects of the HTO procedure on knee joint mechanics. The study researches the impacts of varying the correction angles on the articular surface contact parameters and stress distribution, specifically for under-correction, optimal correction, and overcorrection. Key findings highlight the importance of selecting the appropriate correction angle for HTO for optimal and balanced distribution of load between the medial and lateral compartments, which could be affected if the knee is either undercorrected or overcorrected. Specifically, overcorrecting the knee joint by as little as 2° could potentially increase the risk of complications such as excessive MCL strains leading to damage of the ligament, and further progression of OA even after correction due to abnormal loading patterns. The increase in loading and pressures on the lateral side by overcorrecting could potentially lead to lateral compartment OA. The overall joint stability of the knee could potentially be worsened by compromising the integrity of the MCL. Optimizing the methodology for determining the optimal correction angle is a crucial step to prevent or minimize complications associated with the surgery.

In addition to optimizing correction angles, the study provides insights into modifying the surgical procedure for a better understanding of patient-specific outcomes. The study delves into assessing whether releasing the MCL is a viable option during surgery to further manage symptoms. Depending on the severity of the OA, surgeons could potentially assess the feasibility of releasing the MCL, and if they decide to do so, a decision could be made whether to partially release it or completely release it. The study also provides evidence of the feasibility of a double osteotomy over a single osteotomy for larger corrections. This is particularly valuable for patients with complex deformities and for those who do not achieve satisfactory results with a single osteotomy. Targeting key aspects such as these could help surgeons decide if modifying the procedure is beneficial for better patient outcomes and reduced likelihood of revision surgeries.

Overall, the study provides a non-invasive method to quantitatively assess the biome-

chanical impacts of the surgery and could be used as a potential pre-operative planning tool that extends beyond just the determination of optimal correction. The study could also help optimize postsurgical rehabilitation to help patients achieve improved long-term outcomes.

Chapter 6

Conclusions

6.1 Summary

In this study, FE models were developed to investigate the impact of varying correction angles on the knee joint following a medial opening wedge HTO procedure. The models were constructed based on a clinically relevant approach to determine the optimal surgical correction, building upon previous modeling efforts by [72]. The FE analyses quantified knee contact parameters and stress distributions across the articular surface for scenarios of under-correction, optimal correction, and overcorrection. Additionally, MCL strain was measured to assess its relationship with correction angles and its effects on load and pressure distributions across the articular surface. The potential intervention of MCL release was also examined. Finally, the outcomes of single-level osteotomy were compared with those of double osteotomy for a large correction.

The osteotomy cuts were modeled on 3D models of the tibia and femur using Solidworks, then exported and meshed in Hypermesh. The models were subsequently transferred to Abaqus CAE, where they were assembled with the other knee components. Appropriate loads and boundary conditions were applied to determine the contact parameters. The results showed that contact forces and pressures decreased in the medial compartment and increased in the lateral compartment as the correction angles increased. The stress distribution across the articular surface exhibited a similar trend, and the results were verified against published literature. A balanced distribution of load and pressure between the medial and lateral compartments was observed with a 5° correction, validating the preplanning procedure.

The strain in the MCL was quantified as a function of force in the spring elements. The model confirmed the hypothesis that MCL strain increases with an increase in correction angles. The total force in the MCL spiked in the overcorrected model, resulting in abnormal load distributions on the medial side. An effective method to unload the medial compartment was to release the MCL. With the partial and total release of the superficial MCL, the medial compartment experienced a decrease in load and pressure distributions, demonstrating that MCL release can be an effective option for unloading the medial compartment.

A comparison between the results of single osteotomy and double osteotomy was made on a 7° correction. For larger corrections, a double osteotomy procedure proves to be a viable option to unload the medial compartment, without altering the mechanics of the lateral compartment.

The study highlights the impact of a medial opening wedge HTO on knee joint mechanics following the procedure. A detailed approach to emulate a clinical scenario was adopted to predict and investigate the implications and outcomes. The study shows that FE models can accurately predict the outcomes of surgical procedures, allowing for appropriate pre-planning and post-surgical rehabilitation to minimize complications and improve patient outcomes.

6.2 Limitations and Future Work

Several limitations were identified in this study, which can pave the way for future work, including:

1. The FE models were developed on a 3D model of the knee joint that does not include the hip and ankle joints. The pre-planning procedure for determining the optimal correction was done using a radiograph that does not belong to the knee joint. The involvement of hip and ankle joints in pre-planning procedures and developing a model is crucial for HTO procedures. Future models could be developed by modeling the hip and ankle joints to better predict the knee joint behavior for varying corrections.

2. The material behaviors of soft tissue components like cartilage and menisci are assumed to be linear isotropic. While this assumption has yielded promising results, the accuracy of tibiofemoral contact forces and pressures could be enhanced by accounting for their non-linear behavior. To further improve this study, incorporating non-linearity in FE models for biological systems could produce more realistic results.

3. In addition to the previous limitation, the contact parameters of the articular surface were determined by considering only a single value of Young's modulus for the cartilage. Studies have reported varying values for the elastic behavior of cartilage. The response in the cartilage models could significantly vary by considering different values. Future research could include a comparative analysis of these varying material behaviors to better predict outcomes.

4. Another limitation also concerns the material behavior of cartilage. The current model uses the material properties of healthy knee cartilage. The study's accuracy could be improved by considering the material behavior of an arthritic knee, providing a better understanding of the behavior of the diseased knee.

5. A non-linear static simulation was performed on the knee joint by only applying a single load. The study does not consider the involvement of muscle forces in investigating the knee joint mechanics. This may underestimate the knee joint behavior, particularly the cartilage stresses. The involvement of muscle forces could play an important role in the mechanics of the knee by accurately predicting the cartilage behavior.

6. Although a static simulation does predict the behavior of the knee joint quite accurately, future work could include a dynamic simulation. This could include investigating the articular surface contact parameters for activities such as walking, running, and jumping post-surgery. This would provide a better understanding of the knee joint and can help optimize post-surgical rehabilitation procedures.

References

[1] https://open.oregonstate.education/aandp/chapter/9-6-anatomy-of-selected-synovial-joints/.

[2] J. Agneskirchner, C. Hurschler, C. Wrann, and P. Lobenhoffer. The effects of valgus medial opening wedge high tibial osteotomy on articular cartilage pressure of the knee: a biomechanical study. *Arthroscopy*, 23(8):852–861, Aug 2007.

[3] S. Akizuki, V. Mow, F. Müller, J. Pita, D. Howell, and D. Manicourt. Tensile properties of human knee joint cartilage: I. influence of ionic conditions, weight bearing, and fibrillation on the tensile modulus. *Journal of Orthopaedic Research*, 4(4):379–392, 1986.

[4] S. Akizuki, A. Shibakawa, T. Takizawa, I. Yamazaki, and H. Horiuchi. The long-term outcome of high tibial osteotomy: a ten- to 20-year follow-up. *J Bone Joint Surg Br*, 90(5):592–596, May 2008.

[5] R. Altman, E. Asch, D. Bloch, G. Bole, D. Borenstein, K. Brandt, W. Christy, T. D. Cooke, R. Greenwald, and M. Hochberg. Development of criteria for the classification and reporting of osteoarthritis. classification of osteoarthritis of the knee. diagnostic and therapeutic criteria committee of the american rheumatism association. *Arthritis Rheum*, 29(8):1039–1049, Aug. 1986.

[6] C. Armstrong, W. Lai, and V. Mow. An analysis of the unconfined compression of articular cartilage. *J Biomech Eng*, 106(2):165–173, May 1984.

[7] G. Babis, K. An, E. Chao, J. Rand, and F. Sim. Double level osteotomy of the knee: a method to retain joint-line obliquity. clinical results. *The Journal of Bone and Joint Surgery. American Volume*, 84(8):1380–1388, 2002.

[8] E. M. Badley, J. M. Wilfong, S. Zahid, and A. V. Purruccio. THE STATUS OF ARTHRITIS IN CANADA: NATIONAL REPORT. Aug. 2019.

[9] A. Billings, D. Scott, M. Camargo, and A. Hofmann. High tibial osteotomy with a calibrated osteotomy guide, rigid internal fixation, and early motion. long-term follow-up. *J Bone Joint Surg Am*, 82(1):70–79, Jan 2000. Erratum in: J Bone Joint Surg Am 2000 Mar;82(3):450.

[10] L. Blankevoort and R. Huiskes. Validation of a three-dimensional model of the knee. *Journal of Biomechanics*, 29(7):955–961, 1996.

[11] L. Blankevoort, J. Kuiper, R. Huiskes, and H. Grootenboer. Articular contact in a three-dimensional model of the knee. *Journal of Biomechanics*, 24(11):1019–1031, 1991.

[12] C. Bombardier, G. Hawker, and D. Mosher. THE IMPACT OF ARTHRITIS IN CANADA: TODAY AND OVER THE NEXT 30 YEARS. *Arthritis Alliance of Canada*, 2011.

[13] J. M. Brinkman, P. Lobenhoffer, J. D. Agneskirchner, A. E. Staubli, A. B. Wymenga, and R. J. van Heerwaarden. Osteotomies around the knee. *The Journal of Bone & Joint Surgery British Volume*, 90-B(12):1548–1557, 2008.

[14] J. A. Buckwalter and H. J. Mankin. Articular cartilage: Part I. *Journal of Bone and Joint Surgery*, 79(4):600, Apr. 1997.

[15] J. A. Buckwalter, H. J. Mankin, and A. J. Grodzinsky. Articular cartilage and osteoarthritis. *Instr Course Lect*, 54:465–480, 2005.

[16] V. A. Carranza. Developing a finite element model for evaluating the posterior tibial slope in a medial opening wedge high tibial osteotomy. Master's thesis, The University of Western Ontario, 2023.

[17] N. Chandrashekar. *Sex-based difference in the morphology, tensile properties and ultrastructure of the human anterior cruciate ligament and patellar tendon*. Phd thesis, Texas Tech University, Lubbock, TX, USA, 2005.

[18] H. Constantin, L. Salmon, V. Russell, K. Sundaraj, J. Roe, and L. Pinczewski. 20-year outcomes of high tibial osteotomy: Determinants of survival and functional outcome. *The American Journal of Sports Medicine*, 52(2):344–351, 2024.

[19] D. Cooke, A. Scudamore, J. Li, U. Wyss, T. Bryant, and P. Costigan. Axial lower-limb alignment: comparison of knee geometry in normal volunteers and osteoarthritis patients. *Osteoarthritis and Cartilage*, 5(1):39–47, Jan. 1997.

[20] C. Cooper, S. Snow, T. E. McAlindon, S. Kellingray, B. Stuart, D. Coggon, and P. A. Dieppe. Risk factors for the incidence and progression of radiographic knee osteoarthritis. *Arthritis & Rheumatology*, 43(5):995–1000, May 2000.

[21] M. B. Coventry. Upper tibial osteotomy for osteoarthritis. *J Bone Joint Surg Am*, 67(7):1136–1140, Sept. 1985.

[22] M. B. Coventry, D. M. Ilstrup, and S. L. Wallrichs. Proximal tibial osteotomy. a critical long-term study of eighty-seven cases. *The Journal of Bone & Joint Surgery*, 75(2):196–201, Feb 1993.

[23] M. B. Coventry, D. M. Ilstrup, and S. L. Wallrichs. Proximal tibial osteotomy. a critical long-term study of eighty-seven cases. *The Journal of Bone & Joint Surgery*, 75(2):196–201, Feb 1993.

[24] M. DeRogatis, H. K. Anis, N. Sodhi, J. O. Ehiorobo, M. Chughtai, A. Bhave, and M. A. Mont. Non-operative treatment options for knee osteoarthritis. *Ann Transl Med*, 7(Suppl 7):S245, Oct. 2019.

[25] T. L. H. Donahue, M. L. Hull, M. M. Rashid, and C. R. Jacobs. A finite element model of the human knee joint for the study of tibio-femoral contact. *Journal of biomechanical engineering*, 124(3):273–280, 2002.

[26] T. W. Dugdale, F. R. Noyes, and D. J. Styer. Preoperative planning for high tibial osteotomy. the effect of lateral tibiofemoral separation and tibiofemoral length. *Clinical orthopaedics and related research*, 274:248–64, 1992.

[27] X. Flecher, S. Parratte, J.-M. Aubaniac, and J.-N. Argenson. A 12-28-year followup study of closing wedge high tibial osteotomy. *Clin Orthop Relat Res*, 452:91–96, Nov 2006.

[28] P. J. Fowler, J. L. Tan, and G. A. Brown. Medial opening wedge high tibial osteotomy: How i do it. *Operative Techniques in Sports Medicine*, 20(1):87–92, 2012. The Best Articles over 20 Years.

[29] A. J. S. Fox, A. Bedi, and S. A. Rodeo. The basic science of articular cartilage: structure, composition, and function. *Sports Health*, 1(6):461–468, Nov. 2009.

[30] N. Franulic, J. Muñoz, F. Figueroa, P. Innocenti, and N. Gaggero. Lateral hinge fracture in medial opening wedge high tibial osteotomy: a narrative review. *EFORT Open Rev*, 8(7):572–580, 2023. Published 2023 Jul 3.

[31] Y. Fujisawa, K. Masuhara, and S. Shiomi. The effect of high tibial osteotomy on osteoarthritis of the knee. an arthroscopic study of 54 knee joints. *Orthopedic Clinics of North America*, 10(3):585–608, Jul 1979.

[32] M. Golovakha, W. Orljanski, K. Benedetto, S. Panchenko, P. Büchler, P. Henle, et al. Comparison of theoretical fixation stability of three devices employed in medial opening wedge high tibial osteotomy: A finite element analysis. *BMC Musculoskeletal Disorders*, 15(1):1–12, 2014.

[33] J. Hansen and F. Netter. *Netter's Clinical Anatomy*. ClinicalKey 2012. Saunders/Elsevier, 2014.

[34] K. Hauch, D. Villegas, and T. Haut Donahue. Geometry, time-dependent and failure properties of human meniscal attachments. *Journal of Biomechanics*, 43(3):463–468, 2010.

[35] A. Heijink, A. H. Gomoll, H. Madry, M. Drobnič, G. Filardo, J. Espregueira-Mendes, and C. N. Van Dijk. Biomechanical considerations in the pathogenesis of osteoarthritis of the knee. *Knee Surg Sports Traumatol Arthrosc*, 20(3):423–435, Dec. 2011.

[36] R. W. W. Hsu, S. Himeno, M. B. Coventry, and E. Y. S. Chao. Normal axial alignment of the lower extremity and load-bearing distribution at the knee. *Clinical orthopaedics and related research*, 255:215–27, 1990.

[37] A. Huang, M. Hull, S. Howell, and T. Donahue. Identification of cross-sectional parameters of lateral meniscal allografts that predict tibial contact pressure in human cadaveric knees. *Journal of Biomechanical Engineering*, 124(5):481–489, Oct 2002.

[38] C. K. Hui, L. J. Salmon, A. Kok, and et al. Long-term survival of high tibial osteotomy for medial compartment osteoarthritis of the knee. *The American Journal of Sports Medicine*, 39(1):64–70, 2011.

[39] D. J. Hunter and D. T. Felson. Osteoarthritis. *BMJ*, 332(7542):639–642, 2006.

[40] R. R. Izaham, M. Abdul Kadir, A. Abdul Rashid, M. Hossain, and T. Kamarul. Finite element analysis of puddu and tomofix plate fixation for open wedge high tibial osteotomy. *Injury*, 43(6):898–902, 2012.

[41] J. H. Kellgren and J. S. Lawrence. Radiological assessment of osteo-arthrosis. *Ann Rheum Dis*, 16(4):494–502, Dec. 1957.

[42] T. Koshino, T. Yoshida, Y. Ara, I. Saito, and T. Saito. Fifteen to twenty-eight years' follow-up results of high tibial valgus osteotomy for osteoarthritic knee. *The Knee*, 11(6):439–444, December 2004.

[43] D. C. Lee and S. J. Byun. High tibial osteotomy. *Knee Surgery and Related Research*, 24(2):61–69, Jun 2012.

[44] M. LeRoux and L. Setton. Experimental and biphasic fem determinations of the material properties and hydraulic permeability of the meniscus in tension. *Journal of Biomechanical Engineering*, 124(3):315–321, 2002.

[45] G. Li, J. Gil, A. Kanamori, and S. L.-Y. Woo. A validated three-dimensional computational model of a human knee joint. *Journal of biomechanical engineering*, 121(6):657–662, 1999.

[46] G. Li, O. Lopez, and H. Rubash. Variability of a three-dimensional finite element model constructed using magnetic resonance images of a knee for joint contact stress analysis. *Journal of Biomechanical Engineering*, 123(4):341–346, Aug 2001.

[47] Y. Li, W. Xie, W. Xiao, and D. Dou. Progress in osteoarthritis research by the National Natural Science Foundation of China. *Bone Research*, 10:41, May 2022.

[48] R. F. Loeser. Age-related changes in the musculoskeletal system and the development of osteoarthritis. *Clin Geriatr Med*, 26(3):371–386, Aug. 2010.

[49] M. N. Luís and R. Varatojo. Radiological assessment of lower limb alignment. *EFORT Open Rev*, 6(6):487–494, June 2021.

[50] R. MacDonald, K. Huebner, J. Farr, C. Dunning, A. Getgood, and T. Burkhart. A synthetic bone insert may protect the lateral cortex and fixation plate following a high tibial osteotomy by reducing the tensile strains. *Knee Surg Sports Traumatol Arthrosc*, 28(6):1814–1820, Jun 2020.

[51] A. MacLeod, G. Serrancoli, B. Fregly, A. Toms, and H. Gill. The effect of plate design, bridging span, and fracture healing on the performance of high tibial osteotomy plates: an experimental and finite element study. *Bone Joint Res*, 7(12):639–649, 2018.

[52] T. Matsushita, S. Watanabe, D. Araki, et al. Differences in preoperative planning for high-tibial osteotomy between the standing and supine positions. *Knee Surgery & Related Research*, 33:8, 2021.

[53] B. Miller, B. Downie, E. McDonough, and E. Wojtys. Complications after medial opening wedge high tibial osteotomy. *Arthroscopy*, 25(6):639–646, Jun 2009.

[54] C. Mina, W. J. Garrett, R. Pietrobon, R. Glisson, and L. Higgins. High tibial osteotomy for unloading osteochondral defects in the medial compartment of the knee. *Am J Sports Med*, 36(5):949–955, May 2008.

[55] A. Miniaci, F. T. Franz T. Ballmer, P. M. Ballmer, and R. P. Jakob. Proximal tibial osteotomy: A new fixation device. *Clinical Orthopaedics and Related Research*, 246:250–259, 1989.

[56] K. Moisio, A. Chang, F. Eckstein, J. S. Chmiel, W. Wirth, O. Almagor, P. Prasad, S. Cahue, A. Kothari, and L. Sharma. Varus-valgus alignment: reduced risk of subsequent cartilage loss in the less loaded compartment. *Arthritis Rheum*, 63(4):1002–1009, Apr. 2011.

[57] K. Moore, A. Dalley, and A. Agur. *Clinically Oriented Anatomy*. Online access: Lippincott LWW Health Library: Integrated Basic Sciences Collection. Wolters Kluwer/Lippincott Williams & Wilkins Health, 2013.

[58] J. Morrison. The mechanics of the knee joint in relation to normal walking. *Journal of Biomechanics*, 3(1):51–61, 1970.

[59] E. Moustridi. Predictive simulation of single-leg landing scenarios for acl injury risk factors evaluation. Master's thesis, Feb. 2022.

[60] H. Nakayama, S. Schröter, C. Yamamoto, T. Iseki, R. Kanto, K. Kurosaka, S. Kambara, S. Yoshiya, and M. Higa. Large correction in opening wedge high tibial osteotomy with resultant joint-line obliquity induces excessive shear stress on the articular cartilage. *Knee Surgery, Sports Traumatology, Arthroscopy*, 26(6):1873–1878, 2018.

[61] D. Naudie, R. B. Bourne, C. H. Rorabeck, and T. J. Bourne. The install award. survivorship of the high tibial valgus osteotomy. a 10- to -22-year followup study. *Clinical Orthopaedics and Related Research*, (367):18–27, Oct 1999.

[62] T. Niinimäki, A. Eskelinen, B. Mann, M. Junnila, P. Ohtonen, and J. Leppilahti. Survivorship of high tibial osteotomy in the treatment of osteoarthritis of the knee: Finnish registry-based study of 3195 knees. *J Bone Joint Surg Br*, 94(11):1517–1521, Nov 2012.

[63] H. Ogawa, K. Matsumoto, and H. Akiyama. The prevention of a lateral hinge fracture as a complication of a medial opening wedge high tibial osteotomy: a case control study. *Bone Joint J*, 99-B(7):887–893, Jul 2017.

[64] J. Palmer, A. Getgood, P. Lobenhoffer, R. Nakamura, and P. Monk. Medial opening wedge high tibial osteotomy for the treatment of medial unicompartmental knee osteoarthritis: A state-of-the-art review. *Journal of ISAKOS*, 9(1):39–52, 2024.

[65] D. Pape, J. Duchow, S. Rupp, R. Seil, and D. Kohn. Partial release of the superficial medial collateral ligament for open-wedge high tibial osteotomy. a human cadaver study evaluating medial joint opening by stress radiography. *Knee Surg Sports Traumatol Arthrosc*, 14(2):141–148, Feb 2006.

[66] T. Pehlivanoglu, K. Yildirim, and T. Beyzadeoglu. High tibial osteotomy. In D. D. Nikolopoulos, G. K. Safos, and J. Michos, editors, *Tibia Pathology and Fractures*, chapter 6. IntechOpen, Rijeka, 2020.

[67] E. Peña, B. Calvo, M. Martínez, D. Palanca, and M. Doblaré. Finite element analysis of the effect of meniscal tears and meniscectomies on human knee biomechanics. *Clinical Biomechanics*, 20(5):498–507, 2005.

[68] E. Pena, B. Calvo, M. Martinez, D. Palanca, and M. Doblaré. Finite element analysis of the effect of meniscal tears and meniscectomies on human knee biomechanics. *Clinical Biomechanics*, 20(5):498–507, 2005.

[69] E. Peña, B. Calvo, M. A. Martínez, and M. Doblaré. Effect of the size and location of osteochondral defects in degenerative arthritis. a finite element simulation. *Computers in Biology and Medicine*, 37(3):376–387, 2007.

[70] G. Polat, H. Balcı, M. Çakmak, M. Demirel, C. Şen, and M. Aşık. Long-term results and comparison of the three different high tibial osteotomy and fixation techniques in medial compartment arthrosis. *J Orthop Surg Res*, 12(1):44, Mar 2017. Published 2017 Mar 16.

[71] H. Rao, R. Bakker, S. McLachlin, and N. Chandrashekar. Computational study of extrinsic factors affecting acl strain during single-leg jump landing. *BMC Musculoskeletal Disorders*, 25:318, 2024.

[72] H. R. Rao. Computational Modelling of Knee Tissue Mechanics During Single-Leg Jump Landing. Master's thesis, University of Waterloo, 2020.

[73] J. Robinson, A. Bull, and A. Amis. Structural properties of the medial collateral ligament complex of the human knee. *Journal of Biomechanics*, 38(5):1067–1074, May 2005.

[74] K. Rönn, N. Reischl, E. Gautier, and M. Jacobi. Current surgical treatment of knee osteoarthritis. *Arthritis*, 2011:454873, Apr. 2011.

[75] X. Roothaer. *Multi-scale study of the mechanical behavior of bearing and bone-bearing bones: towards personalization of FE human models*. PhD thesis, 11 2019.

[76] S. Sabzevari, A. Ebrahimpour, M. K. Roudi, and A. R. Kachooei. High tibial osteotomy: A systematic review and current concept. *Arch Bone Jt Surg*, 4(3):204–212, June 2016.

[77] M. Schiraldi, G. Bonzanini, D. Chirillo, and V. de Tullio. Mechanical and kinematic alignment in total knee arthroplasty. *Ann Transl Med*, 4(7):130, 2016.

[78] L. Sharma, J. S. Chmiel, O. Almagor, D. Felson, A. Guermazi, F. Roemer, C. E. Lewis, N. Segal, J. Torner, T. D. V. Cooke, J. Hietpas, J. Lynch, and M. Nevitt. The role of varus and valgus alignment in the initial development of knee cartilage damage by mri: the most study. *Annals of the Rheumatic Diseases*, 72(2):235–240, 2013.

[79] L. Sharma, J. Song, D. Dunlop, D. Felson, C. E. Lewis, N. Segal, J. Torner, T. D. V. Cooke, J. Hietpas, J. Lynch, and M. Nevitt. Varus and valgus alignment and incident and progressive knee osteoarthritis. *Ann Rheum Dis*, 69(11):1940–1945, May 2010.

[80] L. Sharma, J. Song, D. T. Felson, S. Cahue, E. Shamiyeh, and D. D. Dunlop. The role of knee alignment in disease progression and functional decline in knee osteoarthritis. *JAMA*, 286(2):188–195, July 2001.

[81] S. Song, D. Bae, K. Kim, and C. Park. Long-term survival is similar between closed-wedge high tibial osteotomy and unicompartmental knee arthroplasty in patients with similar demographics. *Knee Surg Sports Traumatol Arthrosc*, 27(4):1310–1319, Apr 2019.

[82] A. Surakanti, M. D. Beckler, and M. M. Kesselman. Surgical versus Non-Surgical treatments for the knee: Which is more effective? *Cureus*, 15(2):e34860, Feb. 2023.

[83] Z. Trad, A. Barkaoui, M. Chafra, and J. M. R.S. Tavares. *FEM Analysis of the Human Knee Joint*. Springer Cham, 2018.

[84] Z. Trad, A. Barkaoui, M. Chafra, and J. M. R. S. Tavares. Finite element analysis of the effect of high tibial osteotomy correction angle on articular cartilage loading. *Proceedings of the Institution of Mechanical Engineers, Part H: Journal of Engineering in Medicine*, 232(6):553–564, 2018.

[85] J. van der Woude, S. Spruijt, B. van Ginneken, and R. van Heerwaarden. Distal femoral valgus osteotomy: bone healing time in single plane and biplanar technique. *Strategies in Trauma and Limb Reconstruction*, 11(3):177–186, Nov 2016.

[86] N. van Egmond, G. Hannink, D. Janssen, A. Vrancken, N. Verdonschot, and A. van Kampen. Relaxation of the mcl after an open-wedge high tibial osteotomy results in decreasing contact pressures of the knee over time. *Knee Surg Sports Traumatol Arthrosc*, 25(3):800–807, Mar 2017. Erratum in: Knee Surg Sports Traumatol Arthrosc. 2018 Jan;26(1):354. doi: 10.1007/s00167-017-4628-1.

[87] A. van Wulfften Palthe, N. Clement, O. Temmerman, and B. Burger. Survival and functional outcome of high tibial osteotomy for medial knee osteoarthritis: a 10-20-year cohort study. *Eur J Orthop Surg Traumatol*, 28(7):1381–1389, Oct 2018.

[88] V. B. Virginia Byers Kraus. Static knee alignment and its association with radiographic knee osteoarthritis. *Osteoarthritis and Cartilage*, 15(7):846–847, July 2007.

[89] Y. Wang, Y. Fan, and M. Zhang. Comparison of stress on knee cartilage during kneeling and standing using finite element models. *Medical Engineering & Physics*, 36(4):439–447, 2014.

[90] H. Weinans, M. Siebelt, R. Agricola, S. Botter, T. Piscaer, and J. Waarsing. Pathophysiology of peri-articular bone changes in osteoarthritis. *Bone*, 51(2):190–196, 2012. Osteoarthritis.

[91] Y. Yu, J. Wang, Y. Li, Y. Chen, and W. Cui. Cartilaginous organoids: Advances, applications, and perspectives. *Advanced NanoBiomed Research*, Dec. 2022.

[92] Y. Zhang and J. M. Jordan. Epidemiology of osteoarthritis. *Clin Geriatr Med*, 26(3):355–369, Aug. 2010.

[93] K. Zheng. *The Effect of High Tibial Osteotomy Correction Angle on Cartilage and Meniscus Loading Using Finite Element Analysis*. PhD thesis, 2014-08-31.